Drug Design, Development and Therapy

Dovepress
Taylor & Francis Group

Open Access Full Text Article

ORIGINAL RESEARCH

Molecular Assessment of Traditional Mongolian Medicine Tonglaga-5 in Lactulose Induced Diarrhea: An in vivo Study

Chunli Ma[1,*], Qiqige Buren[1,*], Mutu Eerde[2,*], Ming Qing[3], Xiufang Bao[4], Linyun Zhao[1], Lili Cao[1], Xin Zhang[1], Qigeqi Bai[4], Meiling Chen[4], Mei Hong[1], Yulong Bao[1], Hua Lian[4]

[1]School of Basic Medicine, Inner Mongolia Medical University, Hohhot, Inner Mongolia, 010110, People's Republic of China; [2]Medical Innovation Center for Nationalities, Inner Mongolia Medical University, Hohhot, Inner Mongolia, 010110, People's Republic of China; [3]International Mongolian Hospital of Inner Mongolia, Hohhot, Inner Mongolia, 010065, People's Republic of China; [4]College of Mongolian Medicine, Inner Mongolia Medical University, Hohhot, Inner Mongolia, 010110, People's Republic of China

*These authors contributed equally to this work

Correspondence: Yulong Bao; Hua Lian, Chilechuan Dairy Economic Development Zone, Hohhot, Inner Mongolia Autonomous Region, 010110, People's Republic of China, Tel +86 18698451017; +86 13171029769, Email yulongbao@immu.edu.cn; lianhua81521@163.com

Propose: To elucidate the mechanisms underlying the therapeutic effects of Tonglaga-5 (TLG5) in the treatment of chronic diarrhea.
Methods: The chemical compositions of TLG5 in both in vitro and systemic circulation were analyzed using UPLC-Q/TOF MS^E. Network pharmacology was applied to predict the therapeutic effects of TLG5 on chronic diarrhea. Molecular docking was utilized to assess the binding affinity between key bioactive compounds and their corresponding targets. A total of 24 male Sprague-Dawley (SD) rats were randomly assigned to three groups: control, model, and TLG5 treatment. Corresponding administration included a standard diet, a high-lactose diet of varying concentrations, and TLG5 by gavage during modeling. Transcriptomic analysis was employed to assess gene expression changes in intestinal tissues. Alterations in the intestinal microbiota were evaluated using 16S rRNA sequencing. qPCR and immunohistochemistry technologies were adopted to analyze the expression of genes and proteins associated with intestinal barrier integrity. ELISA was performed to quantify levels of bile acids and short-chain fatty acids (SCFAs).
Results: UPLC-Q/TOF MS^E identified 118 compounds in vitro and 52 in the systemic circulation. Network pharmacological analysis revealed that the in vitro and in vivo components of TLG5 were associated with five core targets and five key compounds, respectively. RNA sequencing analysis showed that TLG5 treatment inhibited the inflammatory pathway. 16S rRNA sequencing demonstrated that TLG5 administration led to an upregulation of beneficial microbial populations and a concomitant downregulation of pathogenic bacteria. The TLG5 treatment group presented a reduction in necrotic areas and inflammatory cell infiltration, as well as preservation of the mucosal structure, with a marked decline in inflammatory lesions. Moreover, TLG5 treatment resulted in a significant increase in the levels of SCFAs and bile acids in the cecum.
Conclusion: TLG5 exerts therapeutic effects on chronic diarrhea through multiple mechanisms, including modulation of intestinal microbiota diversity, enhancement of intestinal barrier function, and attenuation of inflammatory responses.
Keywords: Mongolian medicine Tonglaga-5, chronic diarrhea, intestinal barrier, intestinal microbiota

Introduction

Chronic diarrhea is a prevalent gastrointestinal disorder that affects approximately 17% of the global population.[1,2] With evolving lifestyles and dietary patterns, the incidence of diarrhea-related diseases has been increasing, severely challenging public health worldwide.[3] Chronic diarrhea not only induces persistent abnormal defecation but can also result in malnutrition, dehydration, electrolyte imbalances, and other complications, undermining patients' overall health. Currently, a variety of pharmacological treatments are available for chronic diarrhea, including loperamide, 5-hydroxytryptamine type 3 (5-HT3) receptor antagonists, docusate sodium, probiotics, antispasmodics, and rifaximin. These

Received: 15 April 2025
Accepted: 11 July 2025
Published: 18 July 2025

Graphical Abstract

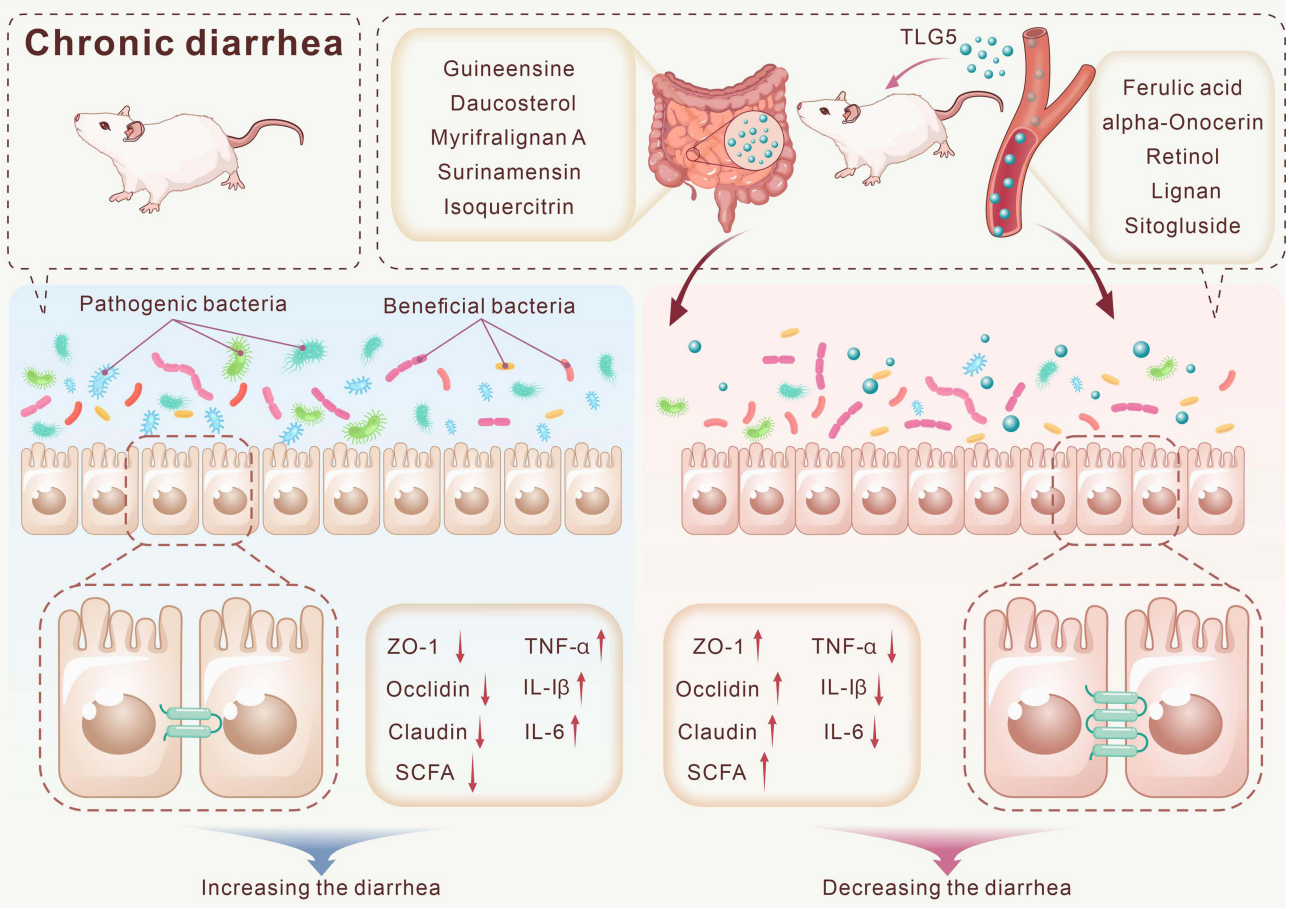

medications exert their effects through diverse mechanisms to alleviate clinical symptoms.[4–6] For example, loperamide, a synthetic opioid agonist, alleviates diarrhea by reducing intestinal motility and inhibiting the loss of fluids and electrolytes.[7] Despite the availability of these treatment options, many patients discontinue the use of existing anti-diarrheal drugs due to various reasons, such as limited efficacy, significant side effects, or the development of drug resistance. Consequently, the exploration of more effective treatment strategies becomes critically important.

Intestinal microbiota dysbiosis plays an essential role in the pathogenesis of chronic diarrhea. Dysbiosis can lead to impaired intestinal immune function and disruption of the intestinal mucosal barrier, processes that are intricately linked to the development of multiple symptoms and gastrointestinal diseases. The integrity of the mucosal barrier has been proven to be closely associated with the onset of inflammation. Increased intestinal permeability is implicated in elevated levels of inflammatory cytokines and the proliferation of pathogenic microorganisms, both of which contribute to the manifestation and exacerbation of diarrhea symptoms.[8–10]

Tonglaga-5 (TLG5) is an empirically formulated Mongolian medicinal compound. Clinically, TLG5 is used to treat symptoms such as anorexia, cold-induced pain in the epigastric region, bloating, and diarrhea, demonstrating satisfying therapeutic efficacy.[11,12] The formulation, comprising long pepper, cinnamon, pomegranate rind, safflower, cardamom, and hawthorn, possesses a mildly warming property. It is designed to regulate the spleen and stomach, tonify the spleen yang, and astringe the intestines to mitigate diarrhea. The formula targets balancing stomach fire and dispelling cold and dampness. Modern pharmacological studies have reported that TLG5 has antimicrobial, anti-inflammatory, smooth muscle relaxant, and antispasmodic effects,[13–15] although the precise mechanisms underlying these actions remain under debate.

This study employed UPLC-Q/TOF MS^E to analyze TLG5 components and applied network pharmacology and molecular docking techniques to identify the effective ingredients of TLG5 and the mechanisms underlying its therapeutic effects on chronic diarrhea. Subsequently, transcriptomic analysis and a rat model of chronic diarrhea were employed to validate the findings. This study unravels the molecular basis of TLG5 in chronic diarrhea treatment, offering theoretical support for the clinical application of TLG5 in managing chronic diarrhea.

Materials and Methods

Materials

TLG5 Preparation

The TLG5 (National Drug Approval No. Z20025218, batch number: 240951) used in this study was purchased from Hohhot Mongolian Medicine and Traditional Chinese Medicine Hospital. This compound preparation is composed of five medicinal materials: cinnamon, pomegranate, long pepper, white cardamom, and safflower. Among them, pomegranate (*Punica granatum* L). (https://www.worldfloraonline.org/taxon/wfo-0000468843), with batch number 2405001, was provided by Hebei Wandong Pharmaceutical Co., Ltd.; white cardamom (*Amomum kravanh* Pierre ex Gagnep). (https://www.worldfloraonline.org/taxon/wfo-0000339068), with batch number C357210302, and long pepper (*Piper Longum* L). (https://www.worldfloraonline.org/taxon/wfo-0000486013), with batch number C790231201, were both provided by Anguo Ronghua Bencao Chinese Medicinal Materials Co., Ltd.; safflower (Carthamus tinctorius L). (https://www.worldfloraonline.org/taxon/wfo-0000024004), with batch number 20140205, was provided by Jinan Renhe Chinese Herbal Decoction Pieces Co., Ltd.; cinnamon (Neolitsea cassia (L). Kosterm).

(https://mpns.science.kew.org/mpns-portal/plantDetail?plantId=2383714andquery=Cinnamomum+cassia+Presl&filter=andfuzzy=falseandnameType=allanddbs=wcsCmp), with batch number 145240801, was provided by Anguo Yuanguang Pharmaceutical Co., Ltd. First, the five medicinal herbs were selected and weighed according to the prescribed formula, ensuring adherence to quality standards. These herbs were then placed in a mortar and ground into a coarse powder. The powder was further pulverized into a fine powder using a grinder, mixed thoroughly, and sieved through a 120-mesh filter. After uniformly mixing by stirring and sieving, the fine powder was packed and stored.

UPLC-Q/TOF-MSE Analysis of TLG5

Approximately 0.5g of TLG5 (Z-FF) and powdered samples of whole pomegranate (QSLiu), cinnamon bark (GPi), white cardamom (BDKou), Piper longum (BBa), and safflower (HHua) were weighed separately and placed in 10 mL volumetric flasks. Methanol was added to the flasks to the 10 mL mark. The mixtures were shaken for 24 hours, followed by ultrasonic treatment for 30 minutes. The samples were then centrifuged at 3000 RPM for 15 minutes. The supernatants were collected and transferred to separate centrifuge tubes, yielding the solutions of each test sample. Subsequently, 50 μL of each test solution was transferred to new tubes, diluted to 1000 μL with the mobile phase (50:50), and filtered through a 0.22 μm membrane. The resulting filtrates were subjected to mass spectrometry analysis.

A total of 20 SPF-grade male Sprague-Dawley (SD) rats, aged 10–12 weeks and weighing 180±20g, were sourced from Beijing Speifo Biotechnology Co., Ltd. (License No. SCXK (Beijing) 2023–0010) and housed at the Animal Center of Inner Mongolia Medical University (temperature: 37°C). After a 7-day acclimatization period, the rats were randomly assigned to the control group and the TLG5 administration group, with ten per group. TLG5 was administered by oral gavage at 40 times a clinical dose for three consecutive days. Prior to the final administration, the rats were fasted for 12 hours (water was allowed). The blood sample was gathered from the ocular orbit of rats at 0.5, 1, 2, 4, 6, 8, 10, 12, and 24 hours post-administration, totaling 2 mL. Post-centrifugation at 3000 rpm for 15 minutes, the serum was obtained and stored at −80°C.

The serum sample was analyzed using UPLC-Q/TOF-MS^E with an ACQUITY UPLC® BEH Shield RP18 column (1.7 μm, 2.1×100 mm, Waters corporation) for separation, with a flow rate of 0.4 mL/min, a column temperature of 40°C, and an injection volume of 2μL. Each time point was analyzed seven times, averaging the results. The mobile phase consisted of 0.1% formic acid (solvent A) and 0.1% formic acid acetonitrile (solvent B), employing gradient elution. Mass spectrometry was performed in electrospray ionization (ESI) mode with optimized spray pressure, auxiliary gas pressure, and other parameters. The m/z scan range was 100–1200.

A custom-built database, which includes chemical components of the constituent herbs (whole pomegranate, cinnamon, white cardamom, cardamom, and safflower) in TLG5 and molecular formulas, was created by reviewing relevant literature. Based on this database and references, raw data were imported into "UNIFI" software using the UPLC-Q/TOF-MS^E technique to screen blood components according to response values and deviations. The final quantitative and qualitative analysis of the test samples and serum was conducted using Waters MassLynx V4.1 and UNIFI software.

Reagents and Instruments

The reagents include The reagents include IL-6 ELISA kit (Neo Bioscience Co., Ltd., ERC003.96), IL-1B ELISA kits (Neo Bioscience Co., Ltd., ERC007.96), TNF-α ELISA kit (Neo Bioscience Co., Ltd., ERC102a.96), rat SCFA kit (Jiangsu MB Biology Co., Ltd., MB-6918A), Masson's trichrome staining kit (Solarbio, G1340), Occludin antibody (Thermo, 33–1500), and Claudin antibody (Thermo, 51–9000).

The instruments encompass a micro refrigerated centrifuge (Thermo, USA), fully-automated rotary microtome (Leica, Germany), fully-automated multifunctional microplate reader (spectra Maxi3x, USA), fluorescence microscope (Leica DM500, Germany), low-temperature incubator for oscillators (FMC-1000, Japan), and mini vertical electrophoresis apparatus (BIO-RAD, USA).

Methodology

Network Pharmacology Analysis

Target Prediction of TLG5 Components

Component collection and database query: Network pharmacology analysis was adopted to predict the targets of 34 TLG5 ingredients isolated from blood, as well as to identify potential targets related to chronic diarrhea, intestinal microbiota imbalance, and inflammation, thereby elucidating the mechanisms of action. The chemical structures of the 34 TLG5 components were retrieved from the PubChem database. Target prediction was then performed using data from the TCMSP (Traditional Chinese Medicine Systems Pharmacology Database), Swiss Target Prediction, and Sea Database.

Prediction of Disease Targets: Target genes associated with chronic diarrhea, intestinal microbiota imbalance, and inflammation were screened from the GeneCards (screening threshold: score ≥ 1), DrugBank, and OMIM databases.[16] The Use of Public Human Database part of this study was approved by by the Ethics Committee of Inner Mongolia Medical University (Ethical approval No.: YKD202405022).

Co-Expression Analysis

The target data on TLG5, chronic diarrhea, intestinal microbiota imbalance, and inflammation were imported into Venn diagram analysis software. Through the intersection analysis of Venn diagrams, key targets co-expressed by TLG5 and these disease states were identified as potential key targets of TLG5 in the treatment of chronic diarrhea and inflammation.

Protein-Protein Interaction (PPI) Network Construction

The intersection target data were uploaded to the String database to construct a PPI network. The species was set to "Homo sapiens", with a confidence threshold of 0.9. A topological analysis of this PPI network was conducted using the Network Analyzer plugin of Cytoscape 3.9 software. Core targets within the network were identified based on calculated node degrees.

Construction of a Compound-Effective Ingredient-Target-Gene Network

In order to elucidate the interactions between effective ingredients, targets, and genes in TLG5, a drug-component-target-gene network was visualized using Cytoscape 3.9. Network analysis was performed to identify key components associated with chronic diarrhea, intestinal microbiota imbalance, and inflammation. The significance of these components was ranked based on their node degrees, with higher degrees indicating greater importance. Components with higher degrees were considered potential key effective ingredients.

Biological Function Enrichment Analysis

GO enrichment and KEGG pathway analyses were performed on the identified targets using the Metascape platform.

Molecular Docking

Molecular docking was employed to evaluate the binding affinity between the active components of TLG5 and their corresponding target proteins. Ten target protein crystal structures, closely associated with chronic diarrhea, were selected from PDB and preprocessed using PyMol. Ligands corresponding to the active components of TLG5 were retrieved from PubChem and optimized in Chem3D for three-dimensional refinement, removal of hydrogen atoms, and preparation for docking. The protein targets were further preprocessed using Autodock 4.4.6 software. Binding affinities between the target proteins and their corresponding ligands were calculated using AutoDock Vina. The docking solution with the lowest binding energy and the optimal binding mode was selected. The binding modes and interaction patterns of the ligands and target proteins were visualized using PyMol software. Ultimately, ligands that may serve as effective therapeutic targets for chronic diarrhea were identified.

Animal Grouping and Model Induction

Following one week of acclimatization, 24 male SD rats (batch no. SCXK(Beijing)2021–0006) were randomly assigned to three groups: a control group, a model group, and a TLG5 treatment group, with eight rats per group. The animal experiment was approved by the Medical Ethics Committee of Inner Mongolia Medical University (Document No.: YKD202405022) and conducted in accordance with the Guide for the Care and Use of Laboratory Animals published by the National Research Council. The control group was maintained on a standard diet, while the model group was fed a diet containing 30%, 40%, and 50% lactose for one week each. In the treatment group, TLG5 was administered via gavage during modeling. Diarrhea was diagnosed based on the observation of watery, soft, yellowish stools, as compared to the normal, well-formed, soft pellets.[17,18]

Drug Administration and Sample Collection

According to clinical usage guidelines, the rat-to-human conversion factor is 7.[19] The standard clinical dose of 9g TLG5 for a 70kg adult human per day was converted to an animal dose of 0.9g/kg, calculated as follows: 9g/70kg x 7 = 0.9g/kg. The treatment group received TLG5 powder suspension at 0.9 g/kg, while the control and model groups were given an equivalent volume of saline (Sichuan Kelun Pharmaceutical Co., Ltd., N23121005) solution for three weeks. Following the final administration, rats were in abrosia for 12 hours with unrestricted water supply. After being weighed, the rats' chest and abdominal skin were disinfected with iodophor. Under anesthesia with 1% pentobarbital sodium via intraperitoneal injection, a midline incision was made to open the skin and abdominal wall muscles, exposing the abdominal cavity. Blood was sampled from the abdominal aorta and left to stand at 4°C. The serum was obtained by centrifugation and aliquoted into sterile centrifuge tubes. Colon tissues were rinsed with physiological saline and divided into two portions: one was fixed in paraformaldehyde, and the other was rapidly frozen in liquid nitrogen and stored at −80°C.

Biochemical Analysis

Detection of IL-1β, IL-6, and TNF-α Levels in Serum Using the ELISA Method

Serum levels of IL-1β(Neo Bioscience Co., Ltd., ERC007.96), IL-6(Neo Bioscience Co., Ltd., ERC003.96), and TNF-α (Neo Bioscience Co., Ltd., ERC102a.96) were quantified using ELISA kits in accordance with the manufacturer's protocols. Optical density (OD) was determined at 450 nm in a fully-automated multifunctional microplate reader (spectra Maxi3x, USA). Standard curves were constructed to calculate serum levels of IL-1β, IL-6, and TNF-α.

SCFA Quantification

Following euthanasia, the cecal contents of the rats were collected and weighed. An aliquot (9:1, v/w) of the cecal material was mixed with saline under ice-cold conditions, followed by centrifugation at 2500 rpm for ten minutes. The resulting supernatant was collected. The experiment was performed according to the SCFA assay kit (Jiangsu MB Biology Co., Ltd., MB-6918A) instructions. Standard and sample wells were set up. Different concentrations of the standard solution were added to the standard wells (50 μL), while 10 μL of the sample and 40 μL of diluent were dispensed into the sample wells. For both standard and sample wells, 100 μL of horseradish peroxidase (HRP)-conjugated antibody was added into each well, followed by sealing with microplate sealers and incubation at 37°C for 60 minutes. Then, the liquid was discarded. After five wash cycles of the plates, substrates A and B (50 μL each) were added to each well. The reaction was incubated in the dark at 37°C for 15 minutes, then terminated with 50 μL of stop solution. The OD value of each well was determined at 450 nm in a fully-automated

multifunctional microplate reader (spectra Maxi3x, USA). Standard curves were plotted using linear regression, and the curve equation was used to derive SCFA levels.

Bile Acid Quantification

After euthanizing the rats, the cecal contents were collected, weighed, and homogenized with saline (9:1, v/w) under ice-cold conditions. The homogenate was then centrifuged at 2500 rpm for ten minutes, collecting the supernatant for bile acid analysis. Bile acid concentrations were measured using a bile acid assay kit (Nanjing Jiancheng Bioengineering Institute, E003-2-1) according to the provided protocol. Standard, blank, and sample wells were prepared, and 3 μL of distilled water (for the blank), 3 μL of the standard solution, and 3 μL of the sample were added to the corresponding wells. Subsequently, 180 μL of Reagent 1 was added to each well, thoroughly mixed, and incubated at 37°C for five minutes. Afterward, following the addition of 180 μL of Reagent 2, the wells were incubated at 37°C for one minute. The absorbance at 405 nm was measured initially (A0) and after a 3-minute incubation at 37°C (A1). The change in absorbance ($\Delta A = A1 - A0$) was used to calculate the bile acid concentration.

Histopathological Observation

Pathological Condition Observation of Colon Tissues Using HE and Masson Staining

Following euthanasia, colon sections of approximately 0.4 cm were excised and fixed in 4% paraformaldehyde (Baisha Biological Co., Ltd., BL539A) for 24 hours. The tissues were subjected to routine dehydration using gradient ethanol. Upon paraffin embedding, the tissues were sectioned at 4 μm, stained with hematoxylin(BASO, BA4097) and eosin(BASO, BA4098), and mounted with neutral balsam. Microscopic images of the stained sections were obtained using a Leica optical microscope (Leica, Wetzlar, Germany). Histological evaluation was conducted based on the extent of inflammatory cell infiltration (scored from 0 to 3, where 0 indicates minimal infiltration in the lamina propria and 3 denotes full transmural infiltration) and the degree of tissue damage (scored from 0 to 3, where 0 represents no damage and 3 implies significant damage to the deeper layers of the intestinal wall).

For assessment of fibrosis, additional sections of the colon were fixed in 4% paraformaldehyde for over 24 hours, processed similarly with gradient dehydration, paraffin embedding, and sectioned at 4 μm. Masson's kit (Solarbio, G1340) was applied following the manufacturer's protocol. Then, the slides were mounted. Collagenous and muscle fibers were detected to assess fibrosis in the colon tissue.

Immunohistochemical Detection

Freshly excised colon tissues were immediately fixed in 10% neutral-buffered formalin for 24 hours. After dehydration and paraffin embedding, the tissues were sectioned at 4 μm. Then, the sections were baked at 65°C for two hours to enhance adhesion. Following deparaffinization and rehydration, the sections were rinsed using PBS (Fuzhou Maixin Biotechnology Development Co., Ltd., PBS-0060) buffer (pH 7.4) three times, five minutes each, followed by antigen retrieval using citrate (Fuzhou Maxim Biotechnology Co., Ltd., MVS-0101) buffer via heat treatment for four minutes. Next, the sections were cooled naturally at room temperature and washed three times with PBS buffer. Endogenous peroxidase activity was blocked under H_2O_2 treatment for 15 minutes, with subsequent three washes with PBS buffer. Nonspecific binding was minimized by incubating the sections in 5% bovine serum albumin (BSA) for 45 minutes. The primary antibody underwent incubation at 4°C for one night. The next day, after washing the sections three times with PBS, a reaction amplification reagent was applied for 15 minutes, followed by another three PBS washes. The sections were then treated with secondary antibody for 15 minutes and washed three times with PBS. Finally, after DAB (Fuzhou Maxim Biotechnology Co., Ltd., DAB-0031) staining, the sections were dehydrated, mounted, and observed under a microscope fluorescence microscope (Leica DM500, Germany) for imaging.

RT-qPCR Analysis

Total RNA was isolated from colon tissues using Trizol reagent (Lablead, R1000, Beijing). The RNA quality was assessed with a microvolume UV spectrophotometer (Thermo Fisher Scientific, NanoDrop ONE), ensuring an absorbance ratio (260/280 nm) between 1.8 and 2.0 for all samples. Reverse transcription was performed on 1 μg of RNA using gene-specific primers and a reverse transcription kit (TIANGEN, KR118) to obtain first-strand cDNA. RT-qPCR was subsequently carried out on a Roche LightCycler® 480 system (Germany) using SYBR Green dye (TIANGEN, FR217). Relative mRNA expression of target genes was determined using the $2^{\wedge(-\Delta\Delta CT)}$ method, with β-actin as the internal control. The primer sequences are detailed in Table 1.

Table 1 Primer Sequences

Gene	Primer Sequence
Occludin	Downstream Primer: 5'-TCTTCTCGGTTTGGTGGTCT-3'
	Upstream Primer: 5'-CAGCAGCAGTGGTAACTTGG-3'
Claudin-1	Upstream Primer: 5'-GCCCTACTTTGCTGTTCCTG-3'
	Downstream Primer: 5'-CCCTTCCCCCAATTGAGTAT-3'
IL-1β	Upstream Primer: 5'-TGCCACCTTTTGACAGTGATG-3'
	Downstream Primer: 5'-TGATGTGCTGCTGCGAGATT-3'
IL-6	Upstream Primer: 5'-CCAAGAGGTGAGTGCTTCCC-3'
	Downstream Primer: 5'-CTGTTGTTCAGACTCTCTCCCTT-3'
TNF-α	Upstream Primer: 5'-CCCTCACACTCAGATCATCTTCT-3'
	Downstream Primer: 5'-GCTACGACGTGGGCTACAG-3'
HSP90AA1	Upstream Primer: 5'-ATTGCCCAGTTAATGTCC-3'
	Downstream Primer: 5'-ATAGTGAGGGTTCGGTCT-3'
Lcn2	Upstream Primer: 5'-TCTCGATTCCGTCGGGTGGTGG-3'
	Downstream Primer: 5'-CCTGGGTGTCCTGTGTCTG-3'
Ccr7	Upstream Primer: 5'-TGGTCATTTTCCAGGTGTGCT-3'
	Downstream Primer: 5'-TACAGGGTGTAGTCCACGGT-3'
Abcb1b	Upstream Primer: 5'-TCGCTATGCAGATTGGCT-3'
	Downstream Primer: 5'-TAACGCTCGGCAGAATGC-3'
LAMB3	Upstream Primer: 5'-GTATGGCGAGTGGCAGATGA-3'
	Downstream Primer: 5'-GCAGAGAGACAGGGTTCACA-3'
β-actin	Upstream Primer: 5′-ACGCCAACACAGTGCTGTCTG-3′
	Downstream Primer: 5′-TGCTTGCTGATCCACATCTGCTG-3′

16S rRNA Gene Amplicon Sequencing

DNA extraction was performed using the Soil Genomic DNA Extraction Kit (centrifuge column type, Catalog No: DP336). Bacterial diversity was assessed by amplifying the 16S V4 region using primers 341F and 806R. The PCR reaction mixture consisted of 15 μL Phusion High-Fidelity PCR Master Mix, 0.2 μM primers, and 10 ng of genomic DNA template. The amplification conditions included an initial denaturation at 98°C for one minute, followed by 30 cycles of denaturation at 98°C (10 seconds), annealing at 50°C (30 seconds), and extension at 72°C (30 seconds), with a final extension at 72°C for five minutes. The resulting PCR products were purified using magnetic beads. Then, they were quantified and pooled in equal amounts based on concentration. Upon thorough mixing, the PCR products were analyzed, and target bands were excised and recovered. A sequencing library was constructed and quantified with Qubit and qPCR. After confirming the library quality, sequencing was performed. Raw sequencing tags were processed and filtered using the fastp software (Version 0.23.1) to obtain high-quality, clean tags (Bokulich NA et al, 2012). Chimeric sequences were removed to generate valid data. QIIME2 software was used to derive the Chao1 index and annotate species. The Silva 138.1 database was employed for 16S rRNA analysis. β diversity was analyzed based on both weighted and unweighted distances. Through the UPGMA.tre function in QIIME2, a clustering tree was established using the weighted UniFrac distance matrix. Community structure differentiation was identified using Metagenomeseq and LEfSe statistical analyses.

Colonic RNA-Seq Analysis

Total RNA in rat colon tissues was extracted with TRIzol reagent (DP424). RNA integrity and content were determined with the Agilent 2100 Bioanalyzer (Agilent Technologies, CA, USA). mRNA was enriched using Oligo dT magnetic beads. Following fragmentation, first-strand cDNA synthesis was performed with random hexamer primers. Through end repair, adenylate tailing, adapter ligation, fragment selection, amplification, and purification, the cDNA library was constructed. It was quantified using the Qubit fluorometer and RT-qPCR, and its fragment size distribution was analyzed using the Bioanalyzer. Illumina sequencing was conducted to obtain the sequence information of the target fragments. Raw reads were processed using the fastp software. The resulting clean data were analyzed for Q20, Q30, and GC content.[20] The HISAT2 v2.0.5 tool was used to generate the reference genome and align paired-end clean reads to this

genome. Gene prediction was performed with StringTie (1.3.3b) (Mihaela Pertea et al, 2015). Read counts mapped to each gene were obtained using FeatureCounts (1.5.0-p3). FPKM for each gene was obtained from gene length, and the count of mapped reads was determined. Differential gene expression between the control, model, and TLG5 treatment groups was assessed using DESeq2 (1.20.0). Gene set enrichment analysis (GSEA) on GO and KEGG datasets specific to the species was carried out using the GSEA tool (http://www.broadinstitute.org/gsea/index.jsp).

Statistical Analysis

The acquired data have been represented as mean ± standard error of the mean. GraphPad prism 7.04(La Jolla, CA, United States) was used to conduct the statistical analyses. A one-way analysis of variance was applied to the data analysis, and the LSD Multiple Comparison Test was used to evaluate treatment differences. $p < 0.05$ was considered statistically significant. Data are mean ± standard deviation (mean ± SD) of three independent experimental replicates.

Results

Identification of In Vitro and Blood Constituents of TLG5

In Vitro Constituent Analysis

The chemical constituents of TLG5 and its individual herbal components were analyzed using UPLC-Q/TOF MS^E technology. The data were processed using UNIFI software to identify the mass-to-charge ratios (m/z). Based on references, a total of 118 compounds were identified, including 44 in pomegranate, 73 in cinnamon, 70 in white cardamom, 68 in long pepper, and 65 in safflower (Figure 1, Table 2, Figures S1-S5, and Tables S1-S5).

Blood Component Analysis

The chemical components in normal rat serum and TLG5-containing serum at 9 time points post-administration were analyzed. After removing duplicate ones, a total of 52 compounds in blood were detected, comprised of 34 TLG5 ingredients and 18 metabolites. These compounds included alkaloid, terpene, hemiterpene, aldehyde, lignan, phenol, organic acid, glycoside, flavonoid, phenylpropanoid, sesquiterpene, steroid, and alkene (Tables 3, 4, and S6).

Mechanistic Investigation of In Vitro TLG5 Constituents in Ameliorating Chronic Diarrhea Symptoms Through Modulation of Intestinal Microbial Imbalance and Enhancement of Intestinal Barrier Function

Network Pharmacology Analysis of In Vitro TLG5 Constituents in the Treatment of Chronic Diarrhea

Identification of Potential Targets for In Vitro TLG5 Active Constituents

The chemical constituents identified in the five individual medicinal herbs through UPLC-Q/TOF MS^E, alongside the 118 in vitro constituents identified in TLG5, were cross-referenced with components in the TCMS (Traditional Chinese Medicine Systems Pharmacology) database. Following the screening and removal of duplicate targets, a total of 77 active constituents and 1151 associated pharmacological targets were derived (Table S7).

Disease Target Identification

Intestinal microbiota imbalance and compromised intestinal barrier function are crucial pathophysiological contributors to chronic diarrhea. A systematic search was conducted using the keywords “Chronic Diarrhea”, “Dysbiosis”, and “intestinal barrier” in the GeneCards, DrugBank, and OMIM databases. Three target datasets were generated, encompassing 2635 chronic diarrhea-related targets, 309 intestinal dysbiosis-related targets, and 627 intestinal barrier dysfunction-related targets (Table S8).

Intersection-Target Analysis

The 1151 pharmacological targets associated with in vitro TLG5 chemical constituents were analyzed for intersections with the 2635 chronic diarrhea-related targets, 309 intestinal dysbiosis-related targets, and 627 intestinal barrier-related targets. This analysis identified 491 intersection targets associated with chronic diarrhea, 38 related to intestinal dysbiosis, and 126 linked to intestinal barrier dysfunction (Figures 2A–C).

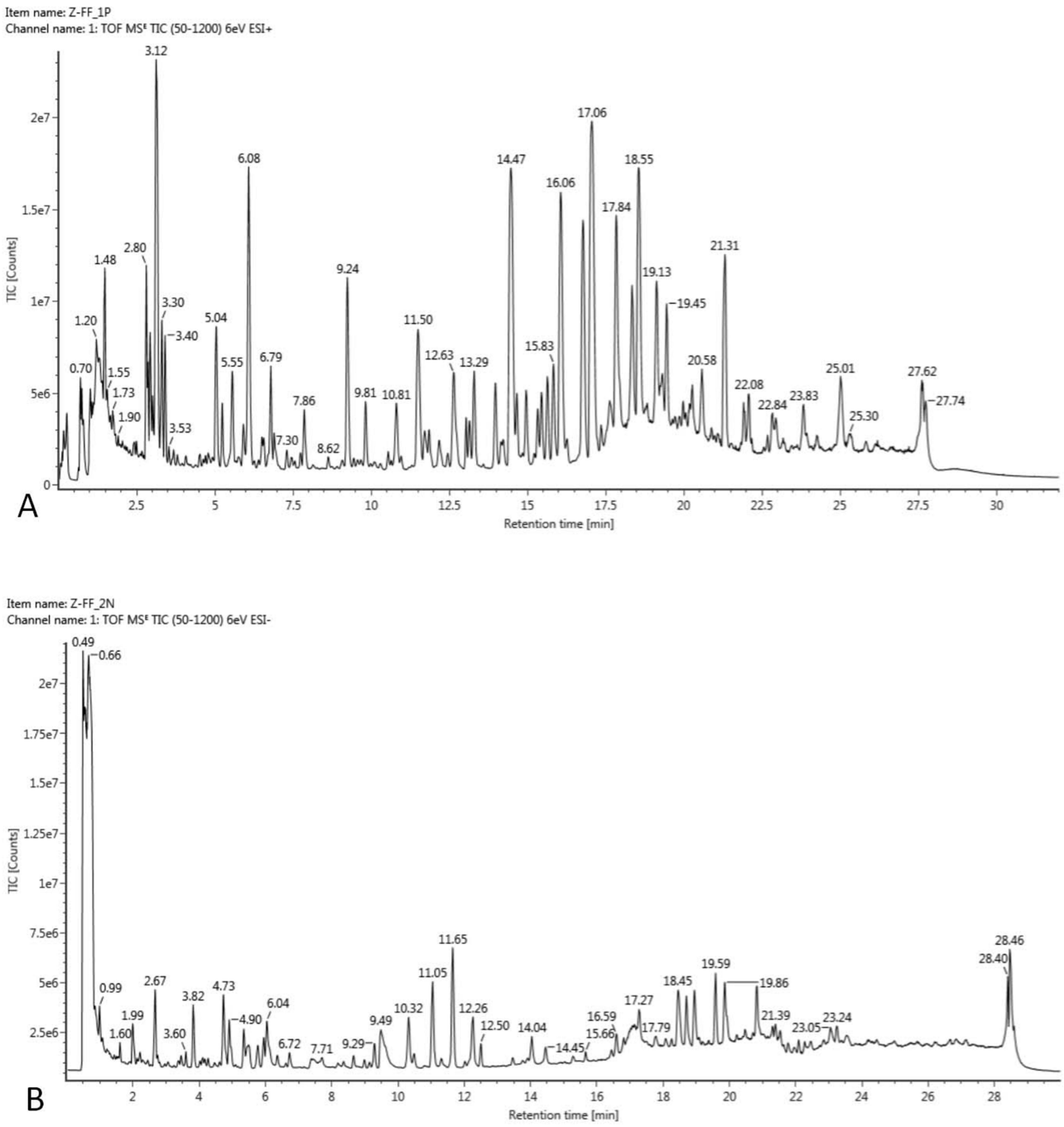

Figure 1 In Vitro Chemical Constituents of TLG5. (**A**) Total Ion Chromatogram (TIC) in positive ion mode. (**B**) TIC in negative ion mode (Z-FF indicates TLG5).

PPI Network Construction and Key Target Screening

The identified intersection targets were imputed to the STRING database to explore their relationships, with a confidence degree of 0.9. The PPI network was constructed using Cytoscape 3.9.1. Topological feature parameters, such as degree centrality, betweenness centrality, and closeness centrality, were calculated using CytoNCA to screen for key genes. Based on degree ranking, the top five key genes linked to chronic diarrhea (TP53, SRC, STAT3, PIK3R1, and PIK3CA), intestinal microbiota imbalance (TNF, NFKB1, IL1B, IL6, and TLR2), and intestinal barrier (STAT3, TNF, AKT1, RELA, and IL6) were identified (Figures 2D–F).

https://doi.org/10.2147/DDDT.S527657

https://doi.org/10.2147/DDDT.S527657

Table 2 In Vitro Chemical Constituents Identification of TLG5

NO.	TR (min)	Selected ion	Formula	Calculated Mass(m/z)	Measured Mass(m/z)	Masserror (ppm)	Detector Counts	Identification	Source
1	17.01	〔M+H〕+ 〔M+Na〕+	$C_{24}H_{43}NO$	362.3416	361.3345	−0.5	4,790,764	(2E,4E,8Z)-N-isobutylicosa-2,4,8-trienamide	D
2	14.43	〔M+H〕+ 〔M+Na〕+	$C_{22}H_{39}NO$	334.3112	333.3032	2.1	4,253,306	(2E,4E,12Z)-N-Isobutylocatadeca-2,4,12-trienamide	H
3	18.56	〔M+H〕+ 〔M+Na〕+	$C_{25}H_{43}NO$	374.3417	373.3345	−0.1	3,624,549	1-[(2E,4E,14Z)-1-Oxo-2,4,14-eicosatrienyl]-piperidine	D
4	16.04	〔M+H〕+ 〔M+Na〕+	$C_{23}H_{39}NO$	346.3109	345.3032	1.4	3,306,172	1-(2E,4E,12E)-Octadecatrinoyl-piperidine	BH
5	16.77	〔M+H〕+ 〔M+Na〕+	$C_{22}H_{41}NO$	336.3262	335.3188	0.4	2755133	N-Isobutyl-2E,4E-octadecadienamide	D
6	3.13	〔M+H〕+ 〔M+Na〕+	$C_{17}H_{19}NO_3$	286.1441	285.1365	1.2	2708360	Piperine	DHGS
7	6.08	〔M+H〕+ 〔M+Na〕+	$C_{21}H_{27}NO_3$	342.2065	341.1991	0.3	2124146	Pipyahyine	B
8	9.24	〔M+H〕+ 〔M+Na〕+	$C_{24}H_{33}NO_3$	384.2533	383.246	−0.2	1657066	Guineensine	DBGS
9	19.13	〔M+H〕+ 〔M+Na〕+	$C_{24}H_{45}NO$	364.357	363.3501	−1	1278108	N-Isobutyl-2E,4E-Decyldecadienamide	DBS
10	18.35	〔M+H〕+ 〔M+Na〕+	$C_{23}H_{41}NO$	348.3265	347.3188	1.1	1235499	Piperoctadecalidine	DHGS
11	1.48	〔M+H〕+ 〔M+Na〕+	$C_{34}H_{37}N_3O_6$	584.274	583.2682	−2.6	1024522	N1,N5-(Z)-N10-(E)-tri-p-coumaroylspermidine	HBD
12	11.5	〔M+H〕+	$C_{18}H_{30}O_2$	279.2324	278.2246	1.9	975,571	9(Z),11(E),13(Z)-Octadecatrienoic Acid	D
13	5.04	〔M+H〕+ 〔M+Na〕+	$C_{14}H_{25}NO$	224.2013	223.1936	1.6	777426	Pellitorine	DBHGS
14	5.56	〔M+H〕+ 〔M+Na〕+	$C_{21}H_{25}NO_3$	340.1909	339.1834	0.6	604541	P(2E,4Z,8E)-N-[9-(3,4-Methylenedioxyphenyl)-2,4,8-Nonatrienoyl]-Piperidine	B
15	12.64	〔M+H〕+ 〔M+Na〕+	$C_{19}H_{38}O_4$	353.2661	330.277	−0.4	598564	L-alpha-Palmitin	DHGS
16	2.8	〔M+H〕+ 〔M+Na〕+	$C_{16}H_{19}NO_3$	274.1445	273.1365	2.5	533468	Piperlonguminine	D
17	6.78	〔M+H〕+ 〔M+Na〕+	$C_{22}H_{29}NO_3$	356.2221	355.2147	0.3	494266	Retrofractamide B	DB
18	7.85	〔M+H〕+ 〔M+Na〕+	$C_{23}H_{29}NO_3$	368.2222	367.2147	0.5	382,808	(2E,4E,10E)-N-11-(3,4-Methylenedioxyphenylhmdecatrienoylpiperidine	DB

19	17.53	(M+H) + (M+Na) +	$C_{24}H_{38}O_4$	413.2661	390.277	−0.4	313827	Macelignan	DHGS
20	5.24	(M+H) + (M+Na) +	$C_{20}H_{27}NO_3$	330.2065	329.1991	0.3	302925	Pipercallosine	DB
21	11.85	(M+H) + (M+Na) +	$C_{26}H_{37}NO_3$	412.2847	411.2773	0.2	293137	Brachystamide B	DB
22	2.81	(M+H) + (M+Na) +	$C_{16}H_{21}NO_3$	276.1598	275.1521	1.3	290595	Dihydropiperlonguminine	DB
23	19.24	(M+H) + (M+Na) +	$C_{26}H_{47}NO$	390.3727	389.3658	−0.9	276,576	(2E,4E,14Z)-N-Isobutyldocosa-2,4,14-Trienamide	DB
24	11.76	(M+H) +	$C_{18}H_{30}O_2$	279.2322	278.2246	1.3	137241	Linolenic acid	DBHG
25	6.8	(M+H) + (M+Na) +	$C_{21}H_{29}NO_3$	344.2222	343.2147	0.6	125946	Piperolein B	B
26	16.7	(M+H) + (M+Na) +	$C_{21}H_{39}NO$	322.3106	321.3032	0.6	114038	Piperlongumine B	-
27	10.55	(M+H) + (M+Na) +	$C_{25}H_{33}NO_3$	396.253	395.246	−0.7	110207	2E,4E,12E,13-(3,4-Methylenedioxyphenyl)-Trideca-Trienoic Acid Isobutylamide	-
28	6.02	(M+H) + (M+Na) +	$C_{15}H_{25}NO$	236.2012	235.1936	1.2	107648	N-[(2E,4E)-Decadienoyl]-piperidine	DBHGS
29	3.1	(M+Na) +	$C_{17}H_{21}NO_3$	310.1413	287.1521	−0.2	104246	Piperanine	H
30	19.13	(M+Na) +	$C_{35}H_{60}O_6$	599.4277	576.439	−0.9	104103	Daucosterol	DHS
31	7.74	(M+H) +	$C_{16}H_{29}NO$	252.2326	251.2249	1.8	93456	2E,4E-N-isobutyl-dodecenamide	DB
32	12.46	(M+H) + (M+Na) +	$C_{19}H_{33}NO$	292.2641	291.2562	2.2	81700	N-[(2E,4E)-Tetradecadienoyl]piperidine	B
33	4.79	(M+H) + (M+Na) +	$C_{20}H_{25}NO_3$	328.1908	327.1834	0.3	78740	Retrofractamide A	B
34	8.63	(M+H) + (M+Na) +	$C_{23}H_{31}NO_3$	370.2378	369.2304	0.4	72694	Piperchabamide B	B
35	10.81	(M+Na) +	$C_{28}H_{48}O_2$	439.3566	416.3654	4.5	63927	Baicalin	HS
36	17.82	(M+H) + (M+Na) +	$C_{40}H_{56}$	537.4481	536.4382	4.8	59892	Lycopene	H
37	14.97	(M+H) +	$C_{18}H_{32}O$	265.2532	264.2453	2.3	53240	Sesquiterpene	DHGS
38	1.21	(M+H) +	$C_{15}H_{10}O_6$	287.055	286.0477	0	52067	Kaempferol_2	DHS
39	10.3	(M+H) + (M+Na) +	$C_{25}H_{35}NO_3$	398.2689	397.2617	−0.3	51,166	(2E,4E,13E)-14-(Benzo[d][1,3]dioxol-6-yl)-Nisobutyltetradeca-2,4,13-trienamide	B
40	1.17	(M+H) +	$C_{15}H_{10}O_7$	303.05	302.0427	0.2	50275	Quercetin	DBHGS
41	3.53	(M+H) +	$C_{13}H_{12}O_4$	233.0812	232.0736	1.8	45552	Methylpiperate	B

(*Continued*)

https://doi.org/10.2147/DDDT.S527657

https://doi.org/10.2147/DDDT.S527657

Table 2 (Continued).

NO.	TR (min)	Selected ion	Formula	Calculated Mass(m/z)	Measured Mass(m/z)	Masserror (ppm)	Detector Counts	Identification	Source
42	2.43	〔M+H〕+ 〔M+Na〕+	$C_{16}H_{17}NO_3$	272.1284	271.1208	1.1	39,494	1-[1-oxo-5(3,4-methylenedioxyphenyl)-2E,4E pentadienyl]-Pyrrolidine	-
43	1.16	〔M+H〕+	$C_{21}H_{20}O_{12}$	465.102	464.0955	−1.7	38087	Isoquercitrin	-
44	3.05	〔M+Na〕+	$C_{12}H_{14}O_4$	245.0786	222.0892	0.8	27707	Diethyl phthalate	DHGS
45	10.14	〔M+H〕+	$C_{19}H_{31}NO$	290.2483	289.2406	1.6	25867	Piperlongumamide C	B
46	6.03	〔M+H〕+	$C_{18}H_{30}O_2$	279.2322	278.2246	1.3	23167	Ligla	DG
47	5.44	〔M+H〕+	$C_{18}H_{16}O_6$	329.1019	328.0947	−0.1	20,787	5-hydroxy-7,3',4'-trimethoxyflavone_1	DG
48	15.99	〔M+H〕+	$C_{20}H_{39}NO$	310.3109	309.3032	1.6	20584	Piperlongimin A	-
49	3.14	〔M+H〕+	$C_{16}H_{19}NO_2$	258.149	257.1416	0.7	18279	Coumaperine	B
50	1.26	〔M+H〕+	$C_{21}H_{20}O_{12}$	465.1014	464.0955	−3	17,453	6-hydroxyka6-hydroxykaempferol-3-O-beta-D-glucoside_1	H
51	10.82	〔M+Na〕+	$C_{27}H_{48}O$	411.3618	388.3705	5	17141	CLR	BGS
52	15.49	〔M+H〕+	$C_{19}H_{32}O_2$	293.2482	292.2402	2.3	17139	Methyllinolenate	HGS
53	9.11	〔M+H〕+	$C_{17}H_{29}NO$	264.2327	263.2249	1.8	15,564	(2E,4E)-N-dodecadienoylpiperidine	S
54	0.73	〔M+H〕+	$C_7H_7NO_2$	138.0552	137.0477	1.9	15558	Trigonelline	HS
55	2.4	〔M+H〕+	$C_{10}H_{10}O_2$	163.0754	162.0681	0	13671	Methyl cinnamate	GS
56	11.51	〔M+H〕+	$C_{21}H_{32}O_2$	317.2475	316.2402	−0.1	12,698	1-(3, 4-Methylenedioxyphenyl) −1E-tetradecene	-
57	2.61	〔M+H〕+ 〔M+Na〕+	$C_{17}H_{19}NO_5$	340.1156	317.1263	0.3	11595	Piperlongumine	D
58	1.76	〔M+H〕+	$C_9H_6O_2$	147.0438	146.0368	−1.7	11442	2H-1-Benzopyran-2-one	G
59	11.5	〔M+H〕+	$C_{10}H_{16}$	137.1325	136.1252	0.1	11087	Sabinene	S
60	16.64	〔M+H〕+	$C_{20}H_{34}O_2$	307.2635	306.2559	1	10581	Sagittariol	HGS
61	3.12	〔M+H〕+	$C_8H_6O_2$	135.0439	134.0368	−1.1	10205	Phenylglyoxal	BG
62	1.41	〔M+Na〕+	$C_{43}H_{42}O_{22}$	933.2051	910.2168	−0.9	9968	Safflower-yellow-A	H
63	6.04	〔M+H〕+	$C_{15}H_{27}NO$	238.2162	237.2093	−1.6	8955	N-Isobutyl-2E,4E-undecadienamide	B
64	1.52	〔M+Na〕+	$C_{21}H_{29}NO_3$	366.2052	343.2147	3.5	8164	(E)-9-(Benzo[d][1,3]dioxol-5-yl)-1-(piperidin-1-yl)non-2-en-1-one	H
65	11.5	〔M+H〕+	$C_{12}H_{18}O_2$	195.1383	194.1307	1.8	7594	1-acetoxy-trans-p-mentha-2,8-diene	S
66	2.28	〔M+H〕+	$C_{14}H_{17}NO_3$	248.1289	247.1208	3.2	7315	Cis-Fagaramide	B
67	2.14	〔M+H〕+	$C_{17}H_{21}NO_3$	288.1596	287.1521	0.5	6931	Feruperine	BGS
68	11.5	〔M+H〕+	$C_{12}H_{18}O$	179.1432	178.1358	0.7	6788	Cyclohexanone,2-Cyclohexylidene-	HGS
69	10.85	〔M+H〕+	$C_{22}H_{33}NO$	328.2637	327.2562	0.6	6786	Piperlongumamide B	B
70	5.62	〔M+H〕+	$C_{15}H_{22}$	203.1795	202.1722	0.4	6617	2-methyl-6-(4-methyl-cyclohexa-1,4-dienyl)-hept-1-ene	DBHSG
71	1.72	〔M+H〕+	$C_{15}H_{10}O_5$	271.0601	270.0528	0.1	5508	Apigenin	-
72	2.19	〔M+H〕+	C_9H_8O	133.0649	132.0575	0.5	5398	Cinnamic aldehyde	DHGS

73	10.82	〔M+H〕+	$C_{14}H_{22}$	191.1796	190.1722	0.8	5222	Germacrene D	BH
74	4.23	〔M+H〕+	$C_{19}H_{23}NO_3$	314.1754	313.1678	1.1	5089	Piperdardine	B
75	2.09	〔M+H〕+ 〔M+Na〕+	$C_{17}H_{23}NO_3$	290.1754	289.1678	1.1	4745	Tetrahydropiperine	-
76	10.81	〔M+H〕+	$C_{15}H_{22}$	203.1794	202.1722	0	4411	Beta-sesquiphellandrene	DBHGS
77	1.29	+Na, +H	$C_{30}H_{30}O_{14}$	637.152	614.1636	−1.2	4341	Safflomin-C	H
78	6.46	〔M+H〕+	$C_{23}H_{41}NO_2$	364.3214	363.3137	1.2	4279	(2E, 4E, 14Z)-6-hydroxyl-N-isobutyleicosa-2,4,14-trienamide	HS
79	11.5	〔M+H〕+	$C_{12}H_{16}$	161.1324	160.1252	−0.4	4111	Thymoquinone	H
80	12.86	〔M+H〕+	$C_{27}H_{39}NO_3$	426.3006	425.293	0.8	3864	Brachystamide D	B
81	13.24	〔M+H〕+ 〔M+Na〕+	$C_{21}H_{40}O_4$	357.3006	356.2927	1.9	3859	(Z)-12-Octadecenic-α-Glycerol Monoester	DHGS
82	1.16	〔M+H〕+	$C_{27}H_{20}O_{18}$	633.0716	632.065	−1	3854	Castalin	S
83	2.4	〔M+H〕+	$C_9H_{10}O$	135.0805	134.0732	0.3	3586	Cinnamyl alcohol	G
84	0.73	〔M+H〕+	$C_5H_{11}NO_2$	118.0865	117.079	2.2	3387	L-Valine	D
85	6.08	〔M+H〕+	$C_5H_{11}N$	86.0966	85.08915	2	2935	Piperidine	S
86	4.59	〔M+H〕+	$C_{14}H_{23}NO$	222.1853	221.178	0.2	2933	Sarmentine	B
87	3.04	〔M+H〕+	$C_9H_{10}O_3$	167.07	166.063	−1.6	2926	Paeonol	HG
88	1.61	〔M+Na〕+	$C_{21}H_{27}NO_3$	364.1898	341.1991	4.2	2885	Pipernonaline	S
89	5.54	〔M+H〕+	$C_{20}H_{29}NO_3$	332.2223	331.2147	0.8	2743	Dehydroretrofractamide C	B
90	0.82	〔M+H〕+	$C_9H_{17}NO$	156.1382	155.131	−0.4	2415	N-Methylisopelletierine	-
91	5.4	〔M+H〕+	$C_{15}H_{22}O$	219.1746	218.1671	1.2	2403	α-Cyperone	DBHG
92	0.98	〔M+H〕+	$C_5H_5N_5$	136.0621	135.0545	2.5	2196	Adenine	-
93	0.72	〔M+Na〕+	$C_{12}H_{22}O_{11}$	365.1052	342.1162	−0.7	2174	Propanetriol-a-arabinofuranosyl(1→4)	G
94	12.64	〔M+H〕+	$C_{16}H_{30}O$	239.2374	238.2297	1.8	1889	Alpha-Bisabolol	DBGS
95	15.53	〔M+H〕+	$C_{28}H_{50}O_6$	483.3686	482.3607	1.3	1826	Myrifralignan A	HG
96	7.93	〔M+H〕+	$C_{15}H_{24}$	205.1951	204.1878	0.3	1817	(+)-DELTA-CADINENE	DHG
97	6.78	〔M+H〕+	$C_{10}H_{14}$	135.1173	134.1096	3.7	1779	Para-menthatriene	G
98	3.8	〔M+Na〕+	$C_{15}H_{22}O_2$	257.1518	234.162	2.2	1676	deca-4,6-diynyl 3-methylbutanoate	BHG
99	20.45	〔M+H〕+	$C_{29}H_{48}O_3$	445.3672	444.3604	−1	1473	Cinnamic acid esters	DHGS
100	6.83	〔M+H〕+	$C_{15}H_{24}$	205.1952	204.1878	0.5	1452	Cyclosativene	DBHG
101	10.65	〔M+Na〕+	$C_{29}H_{56}O_6$	523.3951	500.4077	−3.4	1450	Surinamensin	HGS
102	0.26	〔M+H〕+	$C_{21}H_{36}O_{11}$	465.2307	464.2258	−4.9	1444	Amoenin A3	-
103	14.54	〔M+H〕+	$C_{17}H_{34}O_2$	271.2642	270.2559	3.7	1350	Daturic acid	DHGS
104	0.83	〔M+H〕+	$C_6H_{12}O_6$	203.0529	180.0634	1.6	1182	Aldehydo-D-galactose	-
105	1.54	〔M+H〕+	$C_{15}H_{10}O_7$	303.0496	302.0427	−1.1	1177	6-Hydroxykaempferol	H
106	10.81	〔M+H〕+	$C_{21}H_{20}O_7$	385.1298	384.1209	4.3	1150	(+)-Asarinine	H
107	1.15	〔M+H〕+	$C_{15}H_{14}O_6$	291.0862	290.079	−0.5	1121	Catechin hydrate	SG

(*Continued*)

https://doi.org/10.2147/DDDT.S527657

Table 2 (Continued).

NO.	TR (min)	Selected ion	Formula	Calculated Mass(m/z)	Measured Mass(m/z)	Masserror (ppm)	Detector Counts	Identification	Source
108	16.4	〔M+H〕+	$C_{20}H_{36}O_2$	309.2794	308.2715	1.8	1111	Linoleyl acetate	G
109	1.08	〔M+H〕+	$C_7H_6O_3$	139.0391	138.0317	0.6	1098	Salicylic acid	S
110	9.92	〔M+H〕+	$C_{22}H_{31}NO$	326.2488	325.2406	3.1	1040	Piperlongumamide A	-
111	0.76	〔M-H〕-	$C_7H_6O_5$	169.0147	170.0215	0.4	1351	Gallic acid	S
112	2.95	〔M-H〕-	$C_{30}H_{48}O_4$	473.3641	474.3709	0.4	1610	(2beta,3alpha)-2,3-Dihydroxy-urs-12-en-28-oic acid	S
113	0.84	〔M-H〕-	$C_{15}H_{10}O_6$	285.0404	286.0477	−0.1	1767	Kaempferol	DHS
114	0.75	〔M-H〕-	$C_{16}H_{14}O_6$	301.1642	302.1729	−1.5	2549	6-Hydroxynaringenin	-
115	1.61	〔M-H〕-	$C_{30}H_{50}O$	485.4719	486.4801	−0.9	2761	Lupeol	B
116	1.02	〔M-H〕-	$C_{15}H_{10}O_6$	285.0401	286.0477	−0.3	11327	Scutellarein	DHS
117	10.3	〔M-H〕-	CH_3COOH	281.2482	282.2559	−0.5	18220	Elaidic Acid	DGBHS
118	11.04	〔M-H〕-	$C_{18}H_{30}O_2$	277.2169	278.2246	−0.4	299,320	α-Linolenic acid	DGBHS

Note: "S" is whole pomegranate, "G" is cinnamon, "D" is cardamom, "B" is wickerwork. "H" is saffron, "-" is of unknown origin.

https://doi.org/10.2147/DDDT.S527657

Table 3 Ingredients Chemical Components of TLG5-Containing Serum

	NO	TR (min)	Selected ion	Formula	Calculated Mass(m/z)	Fragmentation	Detector Counts	Identification	Source
Alkaloid	1	13.84	〔M+H〕+	C22H39NO	333.3027	121.10118	1030	(2E, 4E, 12Z) -N-Isobutylocatadeca-2, 4, 12-trienamide	S, G, B, H
	2	16.32	〔M+H〕+	C24H43NO	361.33447	–	3603	(2E, 4E, 14Z) -N-Isobutyleicosa-2, 4, 14-trienamide	G, B, H
	3	16.32	〔M+H〕+	C24H43NO	361.3349	105.06988 135.08044	3651	(2E, 4E, 8Z) -N-isobutylicosa-2, 4, 8-trienamide	S, D, H
	4	11.62	〔M+H〕+	C14H18O3	234.12559	135.08044 173.09609 179.10666	1576	(2E, 8E) −11S-tetradecadiene-4, 6-diyne-1, 11, 14-triol	S
	5	0.97	〔M+H〕+	C26H37NO3	411.27734	–	2497	Brachystamide B	D, B
	6	11.62	〔M+H〕+ 〔M+Na〕+	C19H38O4	330.27701	131.07027 313.27372	1319181	L-alpha-Palmitin	S, G, D, H
	7	16.55	〔M+H〕+	C28H50O6	482.36074	–	1369	Myrifralignan A	H, G
	8	15.86	〔M+Na〕+	C24H43NO	363.35012	71.08553 83.08553	1200	N-Isobutyl-2E, 4E-Decyldecadienamide	D, B
	9	12.12	〔M+H〕+	C20H37NO	307.28751	72.04439	24252	N-Isobutyl-2E, 4E-hexadecadienamide	S, G, D, H
	10	15.60	〔M+H〕+	C22H41NO	335.31881	98.06016	38359	N-Isobutyl-2E, 4E-octadecadienamide	S, G, D, H
	11	11.65	〔M+H〕+	C15H27NO	237.20926	165.12739 168.13829 182.15394	984	N-Isobutyl-2E, 4E-undecadienamide	B
	12	17.02	〔M+H〕+	C15H29NO	239.2252	135.11683 137.13248 149.13248	877	Pellitorine	S, G, D, B, H
	13	15.15	〔M+H〕+	C20H39NO	309.30316	72.08078 128.10699 142.12264	58982	Piperlongimin A	S, G, B, H
	14	7.34	〔M+Na〕+	C30H47NO3	469.35559	121.02841	1073	Piperlongumide	B
	15	17.88	〔M+H〕+	C17H19NO5	321.30316	88.07602	710	Piperlongumine B	B
	16	14.94	〔M+H〕+	C23H39NO	345.30316	–	6788	Piperoctadecalidine	S, G, D, B
	17	0.8	〔M+H〕+	C14H23NO	221.17796	–	757	Sarmentine	B
Terpene (chemistry)	18	6.13	〔M+H〕+	C20H28O	284.21402	121.10118 159.11683 173.13248	3613	Retinal	G
	19	11.61	〔M+H〕+	C20H30O	286.22967	171.11683 175.14813 185.13248	2117	Retinol	G, D
	20	18	〔M+Na〕+	C30H50O2	442.38108	–	985	alpha-Onocerin	D

(*Continued*)

Table 3 (Continued).

Sesquiterpenes (chemistry)	21	11.84	〔M+H〕+	C16H30O	238.22967	109.10118 112.08827 123.11683	1531	alpha-Bisabolol	S, G, H
	22	15.79	〔M+H〕+	C15H22O	218.16707	–	1165	α-Cyperone	G, D, B, H
Aldehyde	23	18.77	〔M+H〕+	C29H48O3	444.36035	383.29446	3328	Cinnamic acid esters	H, S
	24	0.89	〔M+Na〕+	C9H8O	132.05751	–	1427	Cinnamic aldehyde	S, G, D, B
	25	1.03	〔M+H〕+	C9H10O	134.07316	117.06988	1283	Cinnamyl alcohol	S, G, D
Lignin	26	4.94	〔M+H〕+	C18H30O2	278.22458	135.08044	1784	Ligla	G, D
	27	16.87	〔M+H〕+ 〔M+Na〕+	C24H38O4	390.27701	121.02841 149.09609	150458	Macelignan	S, G, H
Phenol	28	13.68	〔M+H〕+	C17H34O2	270.25588	71.08553 83.08553 89.05971	1446	Daturic acid	S, G, D
	29	2.01	〔M+H〕+	C7H6O3	138.03169	93.03349 105.03349 121.02841	2678	Salicylic acid	S
Organic acid	30	8.85	〔M-H〕-	C18H36O2	283.2635	265.25369	10736	Stearic acid	H
	31	21.38	〔M-H〕-	C7H6O5	170.02152	134.00094	2183	Gallic acid	S
	32	9.89	〔M+Na〕+	C22H28O6	500.40769	104.06205 105.06988 133.06988	2807	Surinamensin	S, G, H
Glycoside	33	12.92	〔M+H〕+	C20H34O2	306.25588	91.05423 95.08533 105.06988	1381	Sagittariol	S, G, H
Flavonoids	34	2.01	〔M+H〕+	C10H8O3	176.04734	93.03349 121.02841 160.01550	4232	3- (3'4'-Methylenedioxophenyl) -propenal	G, B

Notes: "S" is whole pomegranate, "G" is cinnamon, "D" is cardamom, "B" is wickerwork. "H" is Saffron.

Table 4 Metabolites Chemical Components of TLG5-Containing Serum

	NO.	TR (min)	Selected ion	Formula	Calculated Mass (m/z)	Fragmentation	Detector Counts	Identification
Alkaloid	1	11.86	〔M+Na〕+	$C_{40}H_{38}N_4O_8$	702.26896	–	9027	4, 4-bis (N-feruioyl) serotonin
	2	17.67	〔M+H〕+	$C_{28}H_{42}O_2$	410.31848	205.12231 217.12231 273.18491	10448	Gamma-Tocotrienol
	3	1.89	〔M+H〕+	$C_{16}H_{10}N_2O_2$	262.07423	–	1456	Indirubin
	4	2.08	〔M+H〕+	$C_{17}H_{19}NO_3$	285.13649	135.04406 201.05462	4429	isopiperine
	5	19.5	〔M+H〕+	$C_{27}H_{40}O_{11}$	540.25706	–	1294	Isovaleroxy-hydroxy dihydrovaltrate
Lignin	6	18.61	〔M+H〕+	$C_{10}H_{12}O_2$	164.08383	–	795	Eugenol_1
	7	1.04	〔M+Na〕+	$C_{20}H_{32}O_6$	368.21989	160.10940 251.12779 266.15126	1235	Pluviatilol
	8	10.98	M-H〕-	$C_{25}H_{30}O_8$	458.1941	–	1116	lignan
Phenylpropanoid (antibiotic)	9	6.44	M+H〕+	$C_{16}H_{24}O_6$	312.15729	203.09140 231.12270 240.09923	4018	4, 6-decadiyne-1-O-β-glucopyranoside
	10	17.7	M+H〕+	$C_{15}H_{14}O_2$	150.06808	105.06988 107.08597 135.08127	693	Phenylpropionic acid
Sesquiterpene (chemistry)	11	1.19	〔M+Na〕+	$C_{10}H_{10}O_4$	194.05791	133.02841 135.04406 163.03897	14997	FeruLic acid
	12	11.26	M-H〕-	$C_{11}H_{16}O_2$	163.113	107.05024	2170	2-Methoxy-4-vinylphenol
Organic acid	13	12.12	〔M+Na〕+	$C_{40}H_{40}N_4O_8$	704.28461	665.26059 675.25752 690.26842	3029	N-[2-[5- (β-D-glucosyloxy) −1H-indol-3-yl]ethyl] feruLamide
Steroidogenic acid	14	18.21	〔M+Na〕+	$C_{35}H_{60}O_6$	576.4411	105.06988	1321	Sitogluside
	15	4.9	〔M+Na〕+	$C_{29}H_{50}O$	414.38617	–	566	Sitosterol
	16	19.03	〔M+H〕+	$C_{30}H_{32}O_{14}$	616.17921	281.04445 297.07575 355.06597	11966	Saffloquinoside E
Flavonoids	17	6.9	〔M-H〕-	$C_{15}H_{14}O_6$	353.1994	–	1090	Catechin
Alkenes	18	0.62	〔M+Na〕+	$C_{15}H_{24}$	204.1867	–	−1.1	Farnesene

Notes: "S" is whole pomegranate, "G" is cinnamon, "D" is cardamom, "B" is wickerwork. "H" is Saffron.

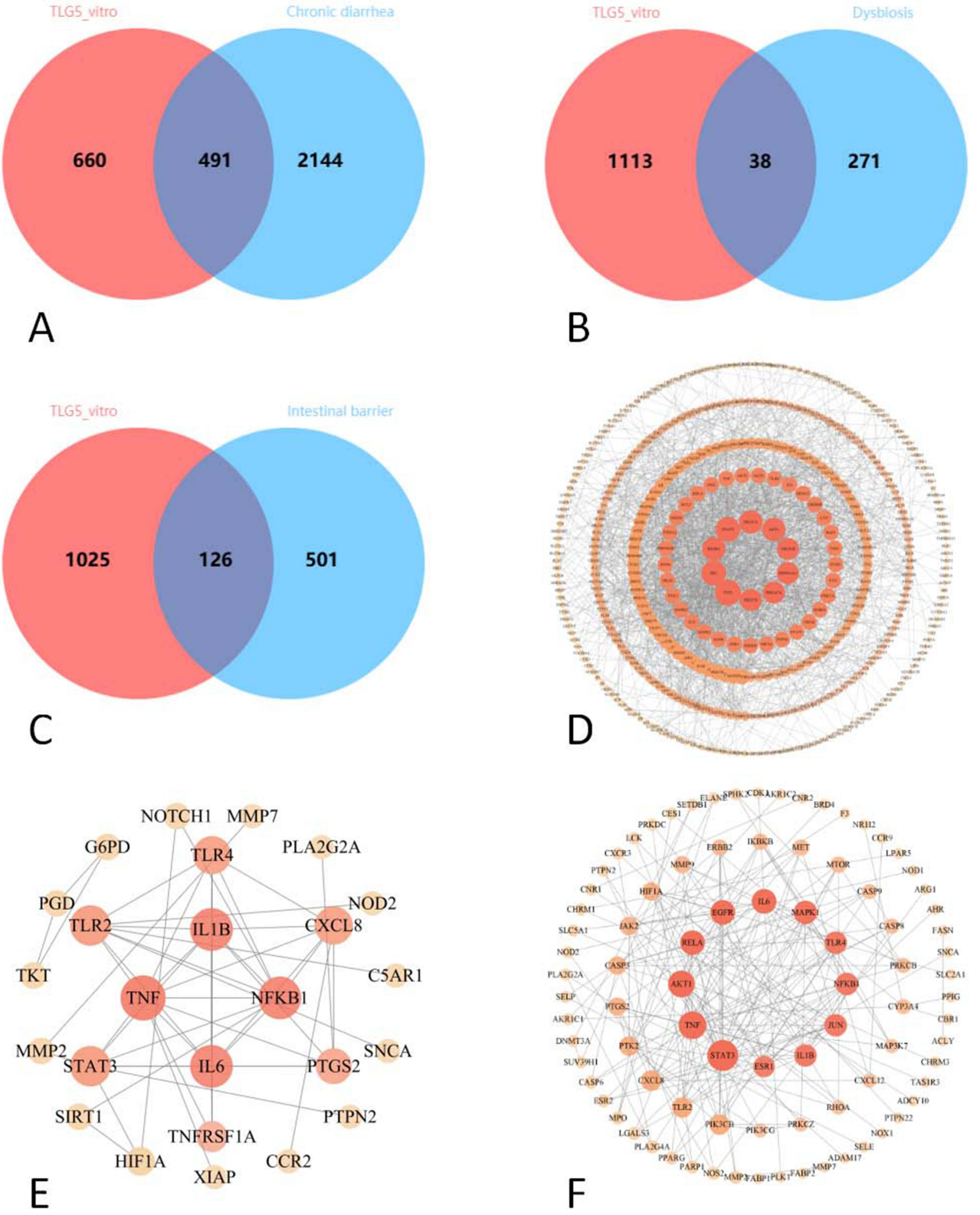

Figure 2 Network Pharmacology of In Vitro TLG5 Constituents in Chronic Diarrhea Treatment. (**A**) Venn diagram of in vitro TLG5 chemical constituent targets and chronic diarrhea disease targets. (**B**) Venn diagram of in vitro TLG5 chemical constituent targets and intestinal microbiota imbalance targets. (**C**) Venn diagram of in vitro TLG5 chemical constituent targets and intestinal barrier function targets. (**D**) PPI network of in vitro TLG5 chemical constituents targeting chronic diarrhea treatment. (**E**) PPI network of in vitro TLG5 chemical constituents targeting intestinal microbiota imbalance treatment. (**F**) PPI network of in vitro TLG5 chemical constituents targeting intestinal barrier treatment.
Notes: Venn diagram ABC shows the number of predicted targets for in vitro components on the left and the number of genes for diseases and symptoms on the right. In PPI network DEF. Lines represent interactions between the targets. The darker the color and the larger the shape, the higher the Degree value.

Construction of In Vitro TLG5 Active Constituent-Intersection Target-Disease Networks

This study established active constituent-intersection gene-disease networks for chronic diarrhea, intestinal microbiota imbalance, and intestinal barrier treatment, respectively. The chronic diarrhea network consists of 491 intersection genes connected to the active constituents of traditional Chinese medicine and disease nodes, containing 606 nodes and 3852 edges. The degree analysis identified the top five active constituents: guineensine, daucosterol, myrifralignan A, surinamensin, and isoquercitrin. The intestinal microbiota imbalance network includes 38 intersection genes linked to the active constituents of traditional Chinese medicine and disease nodes, containing 106 nodes and 324 edges. The degree analysis identified the top five active constituents: elaidic acid, alpha-bisabolol, daturic acid, guineensine, and 9 (Z),11(E),13(Z)-Octadecatrienoic acid. The intestinal barrier network contains 126 intersection genes associated with the active constituents and disease nodes, with 210 nodes and 1227 edges. The degree analysis identified the top five active constituents: guineensine, scutellarein, quercetin, 5-hydroxy-7,3',4'-trimethoxyflavone, and kaempferol. These active constituents are considered key components for subsequent molecular docking (Figures 3A–C).

Functional Enrichment Analysis of Intersection Targets

Functional enrichment of intersection targets associated with chronic diarrhea, intestinal microbiota dysbiosis, and intestinal barrier damage was conducted using the clusterProfiler package, identifying 207 KEGG pathways and 4217 GO terms. The analysis of biological processes (BP) primarily highlighted the following: response to xenobiotic stimulus, response to molecules of bacterial origin, response to decreased oxygen levels, response to hypoxia, and leukocyte migration. Cellular component (CC) analysis indicated enrichment in the membrane microdomain, the external plasma membrane, plasma membrane rafts, secretory granule lumen, and vesicle lumen. Molecular function (MF) enrichment focused on protein tyrosine kinase activity, transmembrane receptor tyrosine kinase activity, protein serine/threonine kinase activity, ligand-activated transcription factor activity, and non-membrane spanning protein tyrosine kinase activity (Figures 4A and B). KEGG analysis revealed the involvement of AGE-RAGE, PI3K-Akt, toll-like receptor, calcium, and chemokine signaling pathways (Figures 4C and D).

Molecular Docking

Key targets, including STAT3, TNF, IL-6, PIK3R1, and PIK3CA, were subjected to molecular docking with five active constituents: guineensine, daucosterol, myrifralignan A, surinamensin, and isoquercitrin (Table S9). Generally, for the absolute value of affinity, > 4.25: average binding activity; > 5.0: good binding affinity; > 7.0: strong binding activity. Consequently, the top five conformations of target proteins included STAT3 vs Daucosterol, TNF vs Isoquercitrin, IL-6 vs Isoquercitrin, PIK3R1 vs Isoquercitrin and PIK3CA vs Daucosterol. These interactions were visualized using Pymol software (Figures 5A–E).

Transcriptomic Analysis of the Regulatory Effect of TLG5 on Intestinal Microbiota and Intestinal Barrier Function

RNA-seq transcriptomic profiling was conducted to probe into the effects and acting mechanisms of chronic diarrhea on colonic tissues. Differential gene expression was analyzed using DESeq2, applying the thresholds of $|\log2(\text{FoldChange})| > 0$ and $\text{padj} < 0.05$. A total of 2074 differentially expressed genes (DEGs) were identified in the model group, with 1058 upregulated and 1016 downregulated. In contrast, the TLG5 treatment group displayed 2813 DEGs, including 1385 upregulated and 1428 downregulated (Figures 6A and B).To validate the accuracy of the transcriptome expression results, we measured the expression levels of 5 randomly selected genes via quantitative real-time PCR: ATP-binding cassette, sub-family B member 1B (abcb1b), C-C Motif Chemokine Receptor 7 (ccr7), LAMININ BETA-3 (Lamb3), Lipocalin-2 (Lcn2) and Tumor Protein P53 (Tp53). The expression patterns of these five genes imply the accuracy of the transcriptome (Figures 6C and D).

KEGG analysis indicated that the downregulated DEGs in the model group were evidently enriched in various pathways related to chronic diarrhea, intestinal microbiota dysbiosis, and intestinal barrier dysfunction. These pathways included bile secretion, focal adhesion, adherens junction, ECM-receptor interaction, MAPK, TGF-β, and protein digestion and absorption. Conversely, the TLG5 treatment group notably activated key signaling pathways involved in

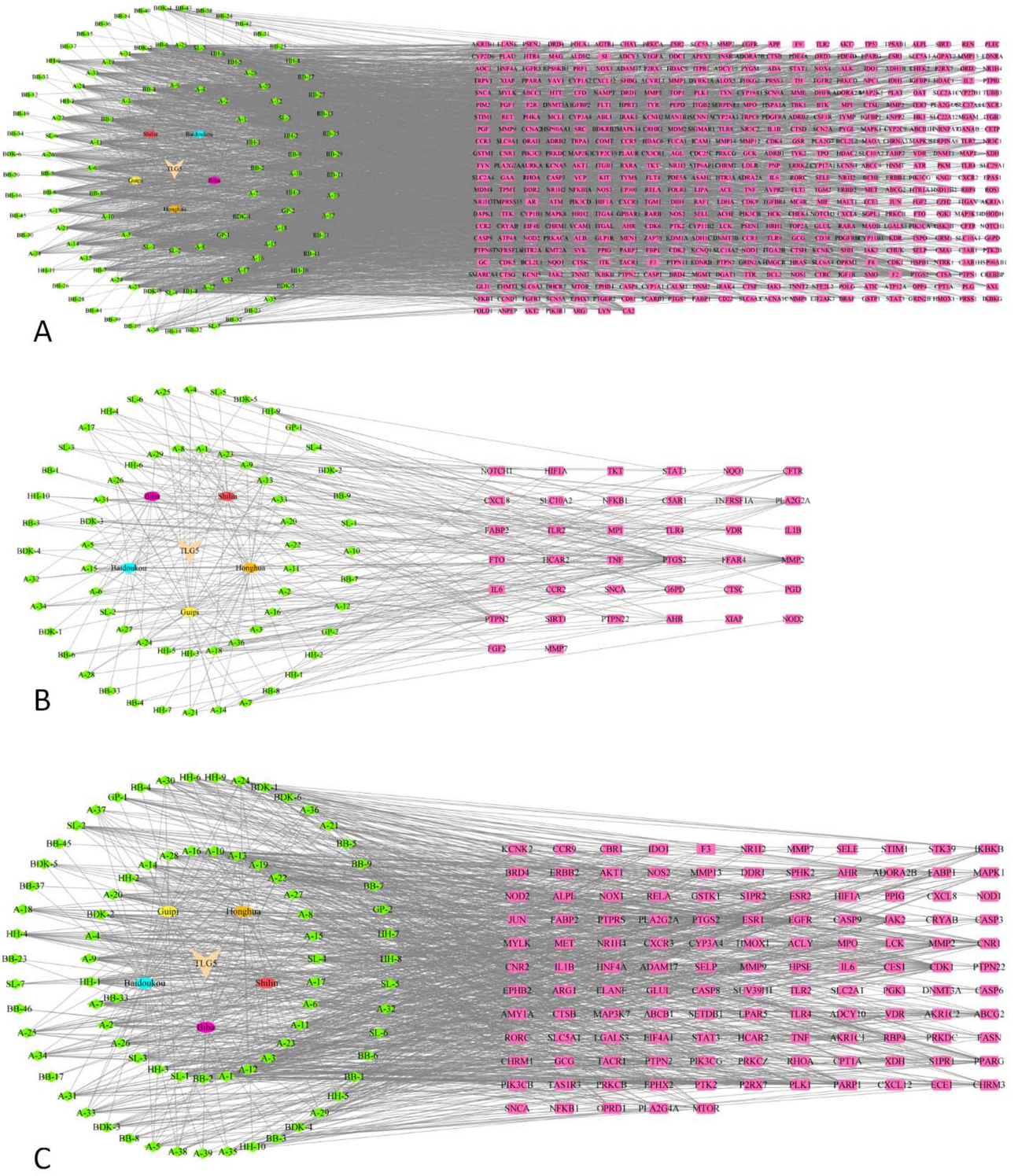

Figure 3 Analysis of In Vitro TLG5 Effective Chemical Constituent-Key Target-Related Disease Networks. (**A**) Analysis of the in vitro TLG5 effective chemical constituent-key target-chronic diarrhea network. (**B**) Analysis of the in vitro TLG5 effective chemical constituent-key target-intestinal microbiota imbalance network. (**C**) Analysis of the in vitro TLG5 effective chemical constituent-key target-intestinal barrier function network.

Notes: In the network analysis diagram, the left circle's center lists the names of the five individual drugs in TLG5, while the surrounding green diamond-shaped area represents their active ingredient targets. On the right, the rectangle displays gene names related to each disease and symptom, with lines depicting the interactions between the ingredients and these conditions.

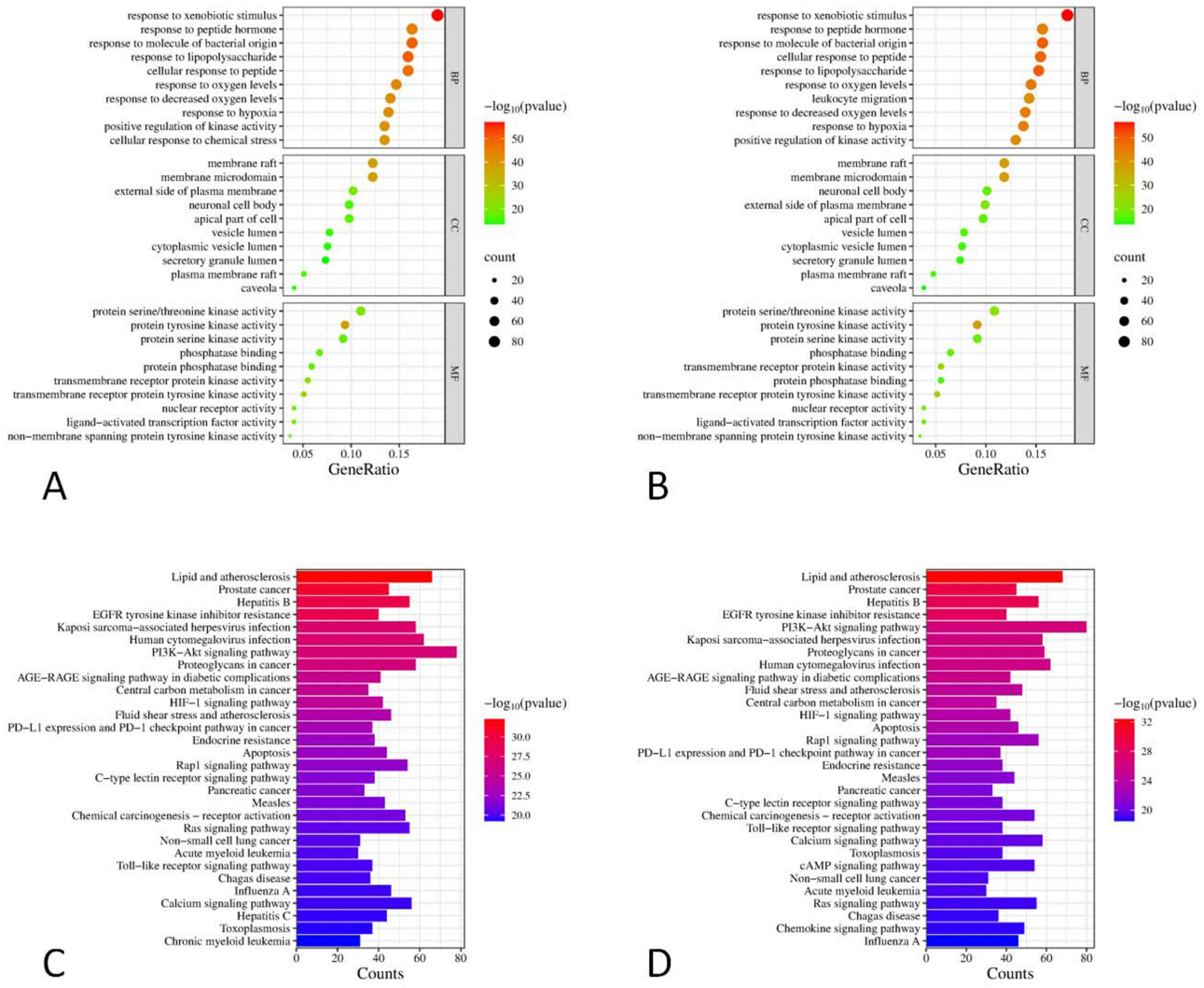

Figure 4 Functional Enrichment and Metabolic Pathway Analysis of In Vitro TLG5 Constituents in Chronic Diarrhea Treatment (and Related Symptoms). (**A**) GO analysis of potential targets of in vitro TLG5 chemical constituents for chronic diarrhea treatment (TOP 10). (**B**) GO analysis of potential targets of in vitro TLG5 chemical constituents for chronic diarrhea and related symptom treatment (TOP 10). (**C**) KEGG analysis of potential targets of in vitro TLG5 chemical constituents for chronic diarrhea treatment (TOP 30). (**D**) KEGG analysis of potential targets of in vitro TLG5 chemical constituents for chronic diarrhea and related symptom treatment (TOP 30).

chronic diarrhea and intestinal barrier function, including bile secretion, mineral absorption, PPAR signaling, fatty acid metabolism, and MAPK signaling (Figures 6E and F).

16S rRNA Sequencing Analysis of the Impact of TLG5 on Intestinal Microbiota Dysbiosis in the Chronic Diarrhea Model

As an oral medication, TLG5 can directly impact intestinal microbiota. In order to explore its specific acting mechanism, 16S rRNA sequencing was performed on the normal rat group, the chronic diarrhea model group, and the TLG5 treatment group. The results showed that the sparse curve showed near saturation, indicating that the sequencing depth of the samples was sufficient to cover most microbial species and that the data were reliable (Figure 7A). The Shannon index was significantly decreased in the model group compared to group C ($p < 0.05$). However, the Shannon index increased in the TLG5 group, but the difference was not statistically significant (Figure 7B). The Venn diagram analysis showed that there were 86 species in the model and C groups, while 130 species overlapped in the model and TLG5 groups. In addition, there were a total of 61 species in the C and TLG5 groups (Figure 7C). Principal Coordinate Analysis (PCoA) revealed differences in clear intergroup flora structure between the control, model, and TLG5 groups (Figure 7D). The effect of TLG5 on the intestinal flora structure of mice with chronic diarrhea showed that TLG5 intervention increased the

https://doi.org/10.2147/DDDT.S527657

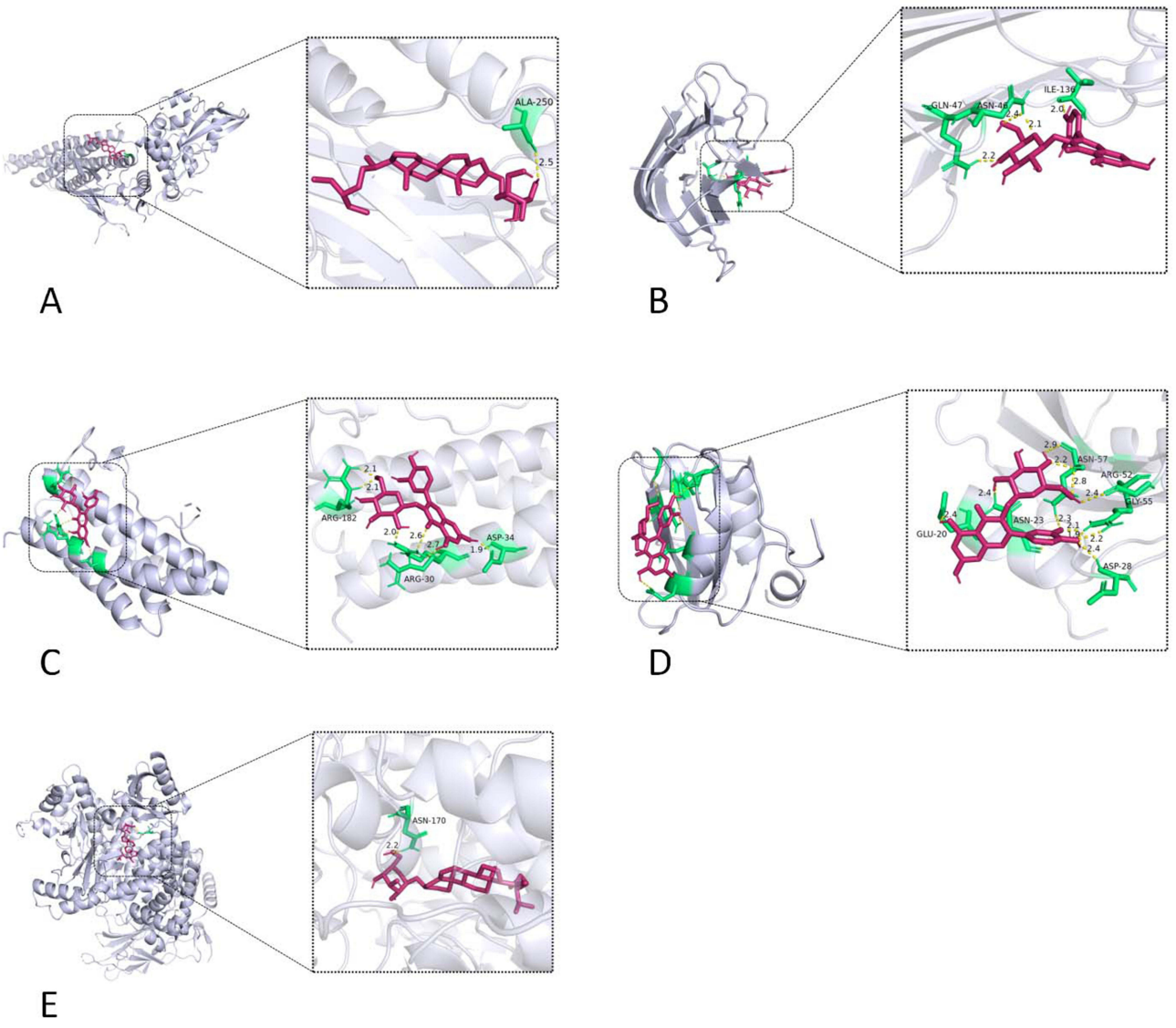

Figure 5 Molecular Docking Results of In Vitro Active Compounds with Key Targets. (**A**) Molecular docking between STAT3 and Daucosterol. (**B**) Molecular docking between TNF and Isoquercitrin. (**C**) Molecular docking between IL-6 and Isoquercitrin. (**D**) Molecular docking between PIK3R1 and Isoquercitrin. (**E**) Molecular docking between PIK3CA and Daucosterol.

Notes: Stick models represent the active molecules, with the green stick structures denoting the carbon backbone of small molecules, red spheres indicating oxygen atoms, white spheres representing hydrogen atoms, and dashed lines depicting the chemical bonds formed between the active compounds and amino acid residues.

abundance of *Bifidobacterium* and *Coriobacteriaceae* UCG-002 at the genus level while decreasing the decrease in the abundance of *Escherichia-Shigella*, compared with the model group (Figure 7E and Table S10). Heat map analysis showed that TLG5 increased the abundance of *Bifidobacterium animalis* and *Clostridium sp*. CL-2 and decreased the abundance of *Bacteroides sartorii* and *Lachnospiraceae bacterium* COE1 (Figure 7F). At the species level, LEfSe results showed major bacteria in each group (Figure 7G).

In Vivo Validation of the Impact of TLG5 on Chronic Diarrhea Symptoms, Intestinal Barrier Function, and Intestinal Microbiota Metabolites

TLG5 Significantly Alleviates Fecal Consistency in Rats with Chronic Diarrhea

As the lactose concentration increased (from 30% to 50%) and the observation period extended (from the first to the third week), the fecal consistency in the control group progressively shifted from severe diarrhea (watery stools with mucus or

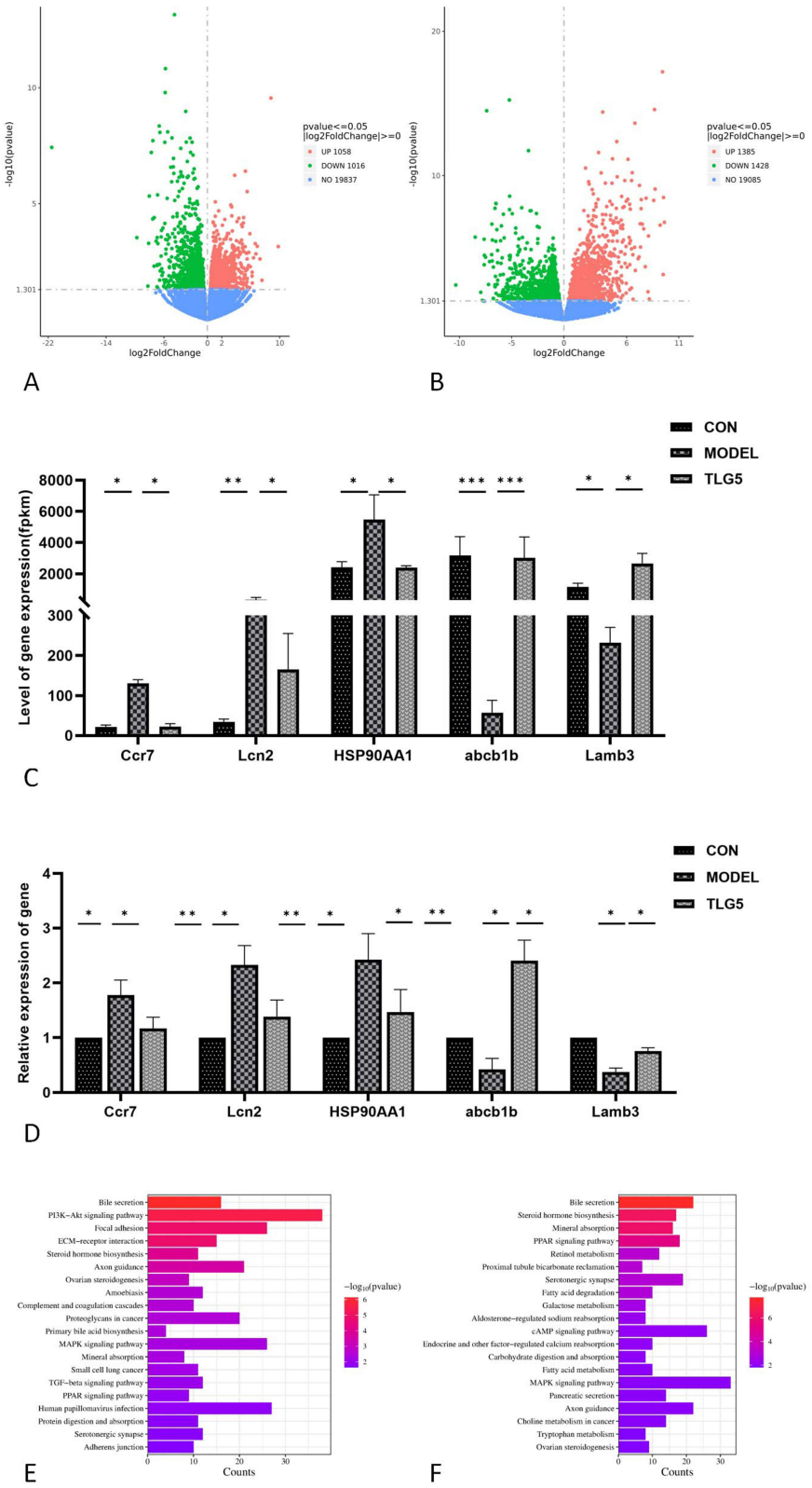

Figure 6 Transcriptomic Analysis of Colon Tissues in Rats with Chronic Diarrhea Treated with TLG5. (**A**) Volcano plot of DEGs between the control group and the model group. (**B**) Volcano plot of DEGs between the model group and the TLG5 treatment group. (**C**) Comparison of the relative fold changes among C, M and TLG5 using RNA-seq (* $p < 0.05$; ** $p < 0.01$, *** $p < 0.001$, n=6). (**D**) Comparison of the relative fold changes among C, M and TLG5 using quantitative real time PCR (* $p < 0.05$; ** $p < 0.01$, n=6). (**E**) KEGG enrichment analysis of downregulated DEGs in the model group compared to the control group. (**F**) KEGG enrichment analysis of downregulated DEGs in the TLG5 treatment group compared to the model group.

Notes: In the volcano plot, the following codes are used: "C" stands for the control group, "M" for the model group, and "TLG5" for the drug treatment group. The map features red dots for upregulated genes, green dots for downregulated genes, and blue dots for genes that do not achieve the significance threshold.

https://doi.org/10.2147/DDDT.S527657

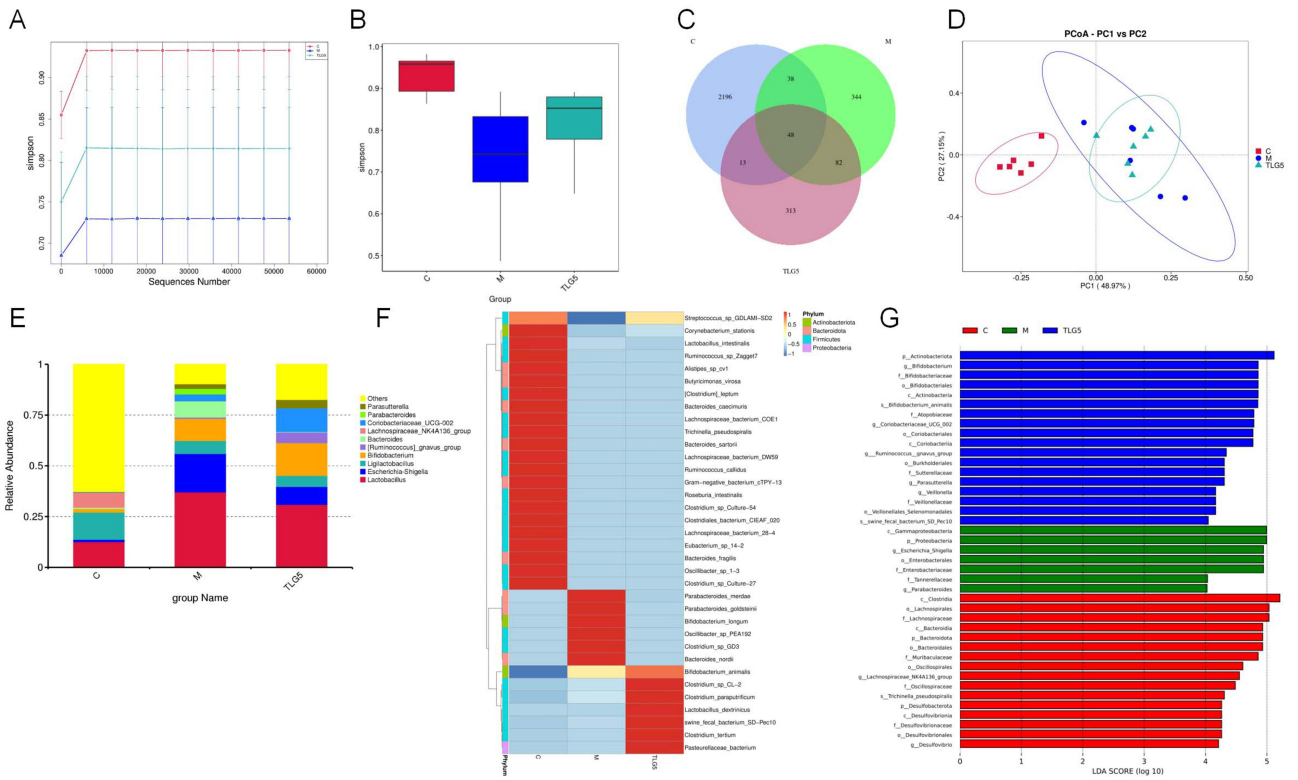

Figure 7 TLG5 improves microbial diversity and genus-specific abundance in rats with chronic diarrhea by remodeling intestinal flora structure. (**A**) Sparse curve analysis. (**B**) Shannon index comparison, (**C**) control group, M: model group, TLG5: TLG5 intervention group. (**C**) Wayne diagram analysis. (**D**) PCoA-based beta diversity. (**E**) Changes in genus-level abundance. (**F**) Heat map analysis: heat maps of relative abundance of species at the species level. (**G**) Histogram of LDA scores based on LEfSe analyses (LDA > 4 was considered to be a differential characteristic taxonomic unit); data are shown as means ± SDs (n = 6), differences between experimental groups were analyzed using a one-way ANOVA, and subsequent analyses were performed using Tukey's multiple comparison test.

loose stools with mucus) to soft, formed pellets. However, even in the 50% lactose diet group, loose stools and mucus remained evident. In comparison, the TLG5 treatment group exhibited milder diarrhea symptoms under identical dietary conditions, with a notably faster recovery in fecal consistency and no occurrence of watery stools and mucus (Table 5).

Table 5 Effect of TLG5 on Faecal Form in Rats with Chronic Diarrhea

Time	Foods	Fecal Forms From 48 Hours to the Third Week				
		Watery Diarrhea + Mucus (Incontinence or Profuse)	Thin Stools + Mucus (Unstructured Stools)	Thin Stools in the Form of Structured Pellets	Softly Formed Pellets	Hardened Plain Pellets
	Standard Foods	–	–	–	+	++++
The first week	30% lactose diet	+++	++++	+	–	–
	TLG5 treatment group	++	++	++	++	–
The second week	40% lactose diet	+++	++	++	–	–
	TLG5 treatment group	+	+	++	++	+
The third week	50% lactose diet	+	++	+	++	–
	TLG5 treatment group	–	+	+	++	+

Notes: Fecal consistency was scored as follows:– (Normal): Formed pellets, dry or slightly moist, non-adherent.+ (Mildly soft): Feces formed but with moist surface, slightly adherent to the perianal area or cage.++ (Moderately loose): Feces unformed (Pasty), visibly adherent to the perianal area or cage, no fluid exudation.+++ (Moderately severe diarrhea): Thick paste with no fixed shape, spontaneous perianal/cage adhesion.++++ (Severe diarrhea): Completely liquid, jetting or extensive anal staining, accompanied by systemic symptoms (Lethargy, weight loss >10%).

These findings suggest that TLG5 plays an essential role in alleviating lactose-induced diarrhea symptoms and promotes the restoration of intestinal function.

TLG5 Repairs Colon Tissues in Rats with Chronic Diarrhea

In order to assess pathological changes in the chronic diarrhea model and the therapeutic effects of TLG5, for rats with chronic diarrhea induced by a high-lactose diet, HE staining and Masson's trichrome staining were performed on their colons before and after TLG5 treatment. Histological examination revealed that, in the control group, the colon mucosa exhibited intact tissue structure with tightly and orderly arranged glands in the mucosal layer, no signs of congestion or edema in the submucosa, and no inflammatory cell infiltration. The boundaries between the longitudinal and circular muscle layers were clear. In contrast, the model group fed a high-lactose diet displayed thinning of the muscular layer, localized ruptures, disorganized cellular arrangement, and considerable infiltration of inflammatory cells without evident collagen deposition. In the TLG5 treatment group, a reduction in necrotic colon area and inflammatory cell infiltration was observed, with the mucosal structure largely intact and the inflammatory region significantly reduced. These results indicate that TLG5 may promote the restoration of cellular integrity in the colon during chronic diarrhea and attenuate the inflammatory response following colonic injury (Figure 8A).

Impact of TLG5 on Intestinal Barrier Function

A compromised intestinal barrier function is recognized as one of the key contributors to the pathogenesis of chronic diarrhea. This study primarily evaluated the potential role of TLG5 in intestinal barrier integrity and assessed tight junction proteins in the colon tissues of rats through experiments. The outcomes revealed a significant reduction in Claudin expression in the colon tissues of rats fed a high-lactose diet in comparison to the control group ($p < 0.05$). Notably, following TLG5 treatment, Claudin expression was substantially upregulated, indicating that TLG5 plays a pivotal role in restoring intestinal barrier function. Similarly, Occludin expression was evidently reduced in the model group. However, the TLG5 treatment group presented higher Occludin expression than the model group ($p < 0.05$), verifying that TLG5 can promote Occludin expression in response to a high-lactose diet (Figure 8B and C).

Histological examination and subsequent analysis showed that ZO-1, Occludin, and Claudin were expressed as brownish-yellow or brown granules within the plasma membrane or cytoplasm of the colon epithelial cells. The intensity of staining was positively correlated with protein expression levels. In the model group, expression levels of ZO-1, Occludin, and Claudin were relatively low. However, following TLG5 treatment, the expression of these three proteins was remarkably enhanced ($p < 0.05$), confirming the role of TLG5 in upregulating their expression (Figure 8D).

Impact of TLG5 on SCFA and Bile Acid Levels in Cecal Contents

The levels of SCFAs and bile acids in cecal contents were quantified to assess the influence of TLG5 on digestive function. The TLG5 treatment group demonstrated a remarkable elevation in SCFA and bile acid levels within the cecum. This suggests that TLG5 not only ameliorates digestive function but also potentially enhances the synthesis of SCFAs and bile acids through modulation of intestinal microbiota metabolism (Figure 8E and F).

Mechanistic Exploration of TLG5 Components in Blood to Alleviate Chronic Diarrhea Symptoms Through Anti-Inflammatory Effects

Network Pharmacology Prediction of Anti-Inflammatory Targets for TLG5 Components in Blood

Inflammation is a major contributor to the pathogenesis of chronic diarrhea. A total of 34 identified TIG5 ingredients in blood were matched with the TCMS database to predict their targets, yielding 32 active components and 638 associated drug targets (Table S11).

Prediction of Disease-Associated Targets

In order to elucidate the inflammatory mechanisms implicated in chronic diarrhea, a comprehensive search was conducted in GeneCards, DrugBank, and OMIM databases using "inflammation" as a keyword. An inflammation-related data set was established, containing 1841 targets (Table S8).

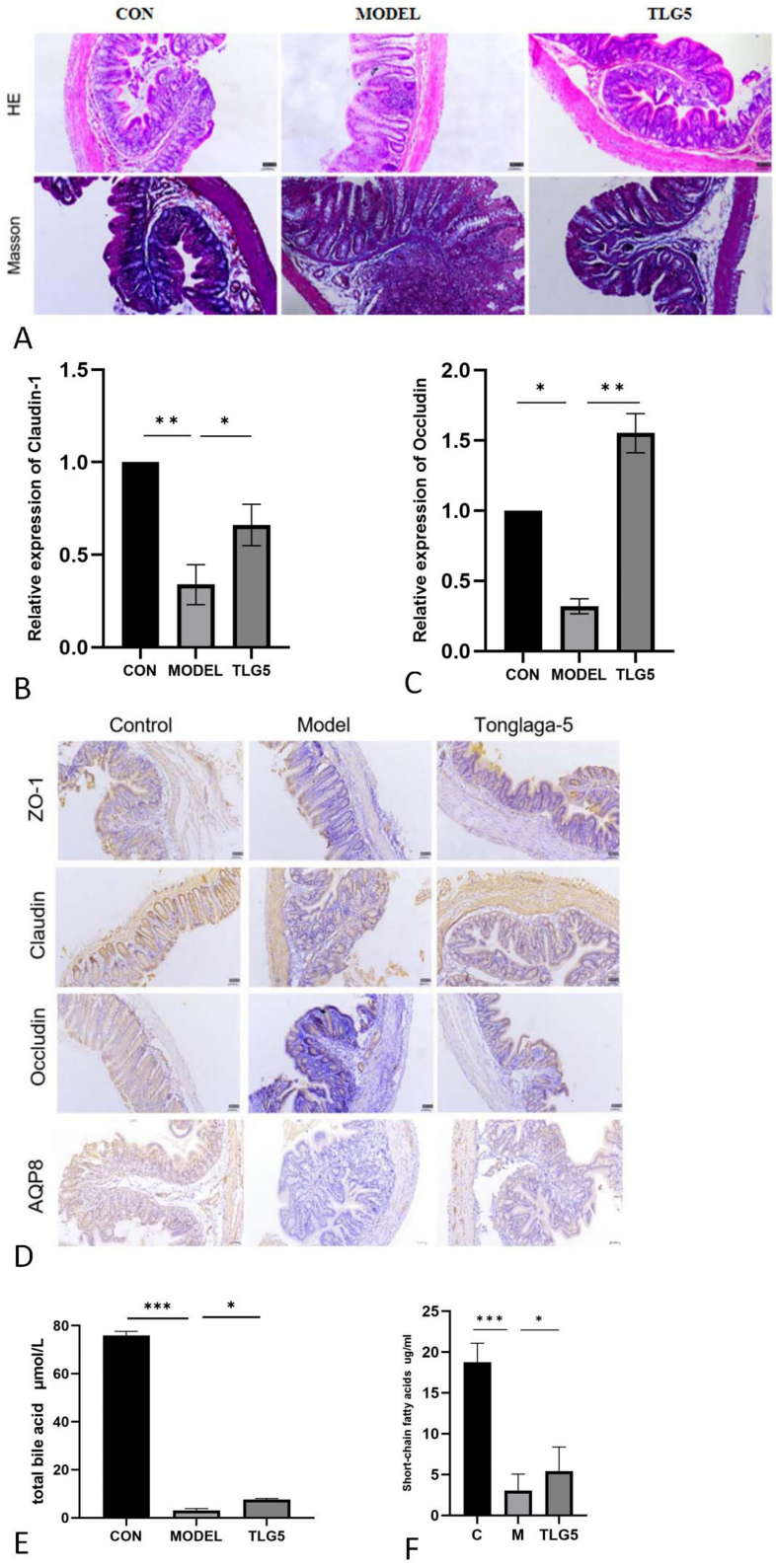

Figure 8 TLG5 Alleviates Chronic Diarrhea Symptoms, Enhances Intestinal Barrier Function, and Modulates Microbial Metabolites. (**A**) HE (×100) and Masson (×100) staining of rat colon tissues. (**B**) qPCR analysis of Claudin mRNA expression, with data presented as mean ± SD (* $p < 0.05$; ** $p < 0.01$, n=6). (**C**) qPCR analysis of Occludin mRNA expression, with data presented as mean ± SD (* $p < 0.05$; ** $p < 0.01$, n=6). (**D**) Immunohistochemical analysis of tight junction proteins (ZO-1, Claudin, and Occludin) in rat colon tissues (×100, n=6). (**E**) ELISA analysis of bile acid levels, with data presented as mean ± SD (* $p < 0.05$; *** $p < 0.001$, n=6). (**F**) ELISA analysis of SCFA levels, with data presented as mean ± SD (* $p < 0.05$; *** $p < 0.001$, n=6).

Intersection-Target Screening

In order to investigate the potential mechanisms through which TLG5 components in blood influence chronic diarrhea and inflammation, an intersection analysis between 638 regulatory targets of the 32 TLG5 active components and 2635 chronic diarrhea-related targets, as well as 1841 inflammation-related targets, was performed. A total of 321 intersection targets related to chronic diarrhea and 212 ones linked to inflammation were obtained (Figures 9A and B).

PPI Network Construction and Key Target Screening

In order to explore the relationships between the intersection targets of chronic diarrhea and inflammation, similar to the above, this study constructed and analyzed a PPI network. Key genes were successfully identified. Based on degree ranking, the top five genes for chronic diarrhea treatment included SRC, PIK3CA, STAT3, HSP90AA1, and PIK3CB. For inflammation treatment, the top five targets were HSP90AA1, AKT1, STAT3, MAPK1, and ESR1 (Figures 9C and D).

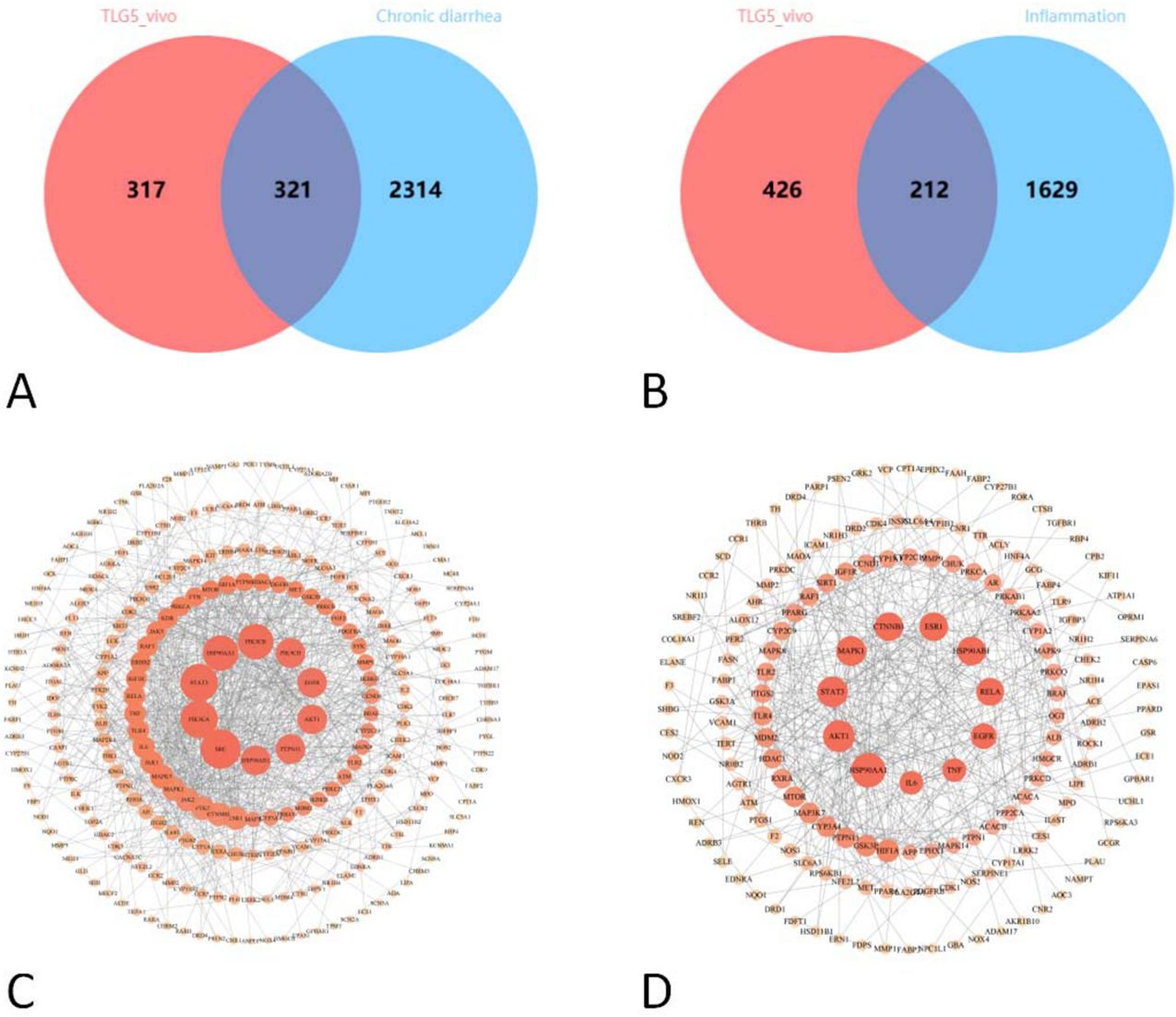

Figure 9 Network Pharmacology Analysis of In Vivo TLG5 Chemical Components. (**A**) Venn diagram of in vivo TLG5 chemical component targets and chronic diarrhea targets. (**B**) Venn diagram of in vivo TLG5 chemical component targets and inflammation targets. (**C**) PPI network of in vivo TLG5 chemical components targeting chronic diarrhea. (**D**) PPI network of in vivo TLG5 chemical components targeting inflammation.

Notes: Venn diagram ABC shows the number of predicted targets for in vitro components on the left and the number of genes for diseases and symptoms on the right. In PPI network DEF. Lines represent interactions between the targets. The darker the color and the larger the shape, the higher the Degree value.

https://doi.org/10.2147/DDDT.S527657

Construction of Networks of TLG5 Active Component in Blood - Intersection Target - Disease

In order to investigate the mechanisms of in vivo TLG5 active components and their relationship to disease, networks of TLG5 active component in blood - intersection target - disease were constructed. The network of chronic diarrhea consisted of 321 intersection genes connected to active components and disease nodes, with 358 nodes and 1012 edges. The degree analysis identified the top five active components: sitogluside, ferulic acid, lignan, alpha-onocerin, and retinol. The inflammation network included 212 intersection genes connected to active components and disease nodes, comprising 249 nodes and 743 edges. The degree analysis revealed the top five active components: ferulic acid, alpha-onocerin, retinol, sitosterol, and sitogluside. These components were selected as key candidates for subsequent molecular docking studies (Figures 10A and B).

Functional Enrichment Analysis of Intersection Targets

Functional enrichment analysis was performed on the 376 intersection targets of chronic diarrhea and inflammation (with a significance threshold of $p < 0.05$), yielding 191 KEGG pathways and 3742 GO terms. In the BP category, the enriched terms involved response to molecules of bacterial origin, response to lipopolysaccharide, response to peptide hormone, positive regulation of the MAPK cascade, and response to nutrient levels. Regarding the CC category, the enriched terms were linked to membrane microdomain, plasma membrane raft, neuronal cell body, vesicle lumen, and protein kinase complex. In terms of MF, the enriched terms were related to protein serine/threonine kinase activity, protein tyrosine kinase activity, transcription coregulator binding, steroid binding, and histone kinase activity (Figures 11A and B).

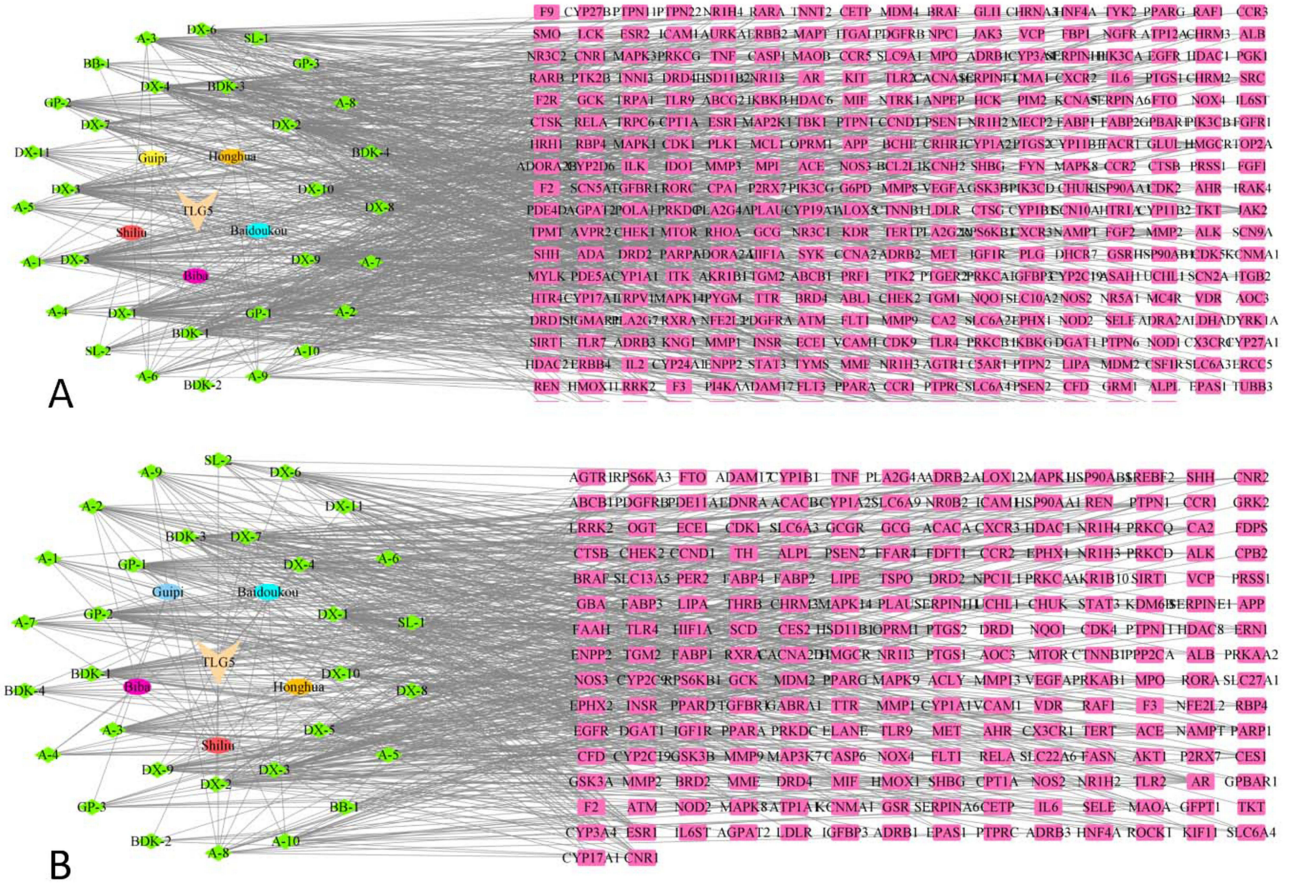

Figure 10 Analysis of In Vivo TLG5 Active Component - Key Target - Associated Disease Networks. (**A**) Analysis of the in vivo TLG5 active component - key target - chronic diarrhea network. (**B**) Analysis of the in vivo TLG5 active component - key target - inflammation network.

Notes: In the network analysis diagram, the left circle's center lists the names of the five individual drugs in TLG5, while the surrounding green diamond-shaped area represents their active ingredient targets. On the right, the rectangle displays gene names related to each disease and symptom, with lines depicting the interactions between the ingredients and these conditions.

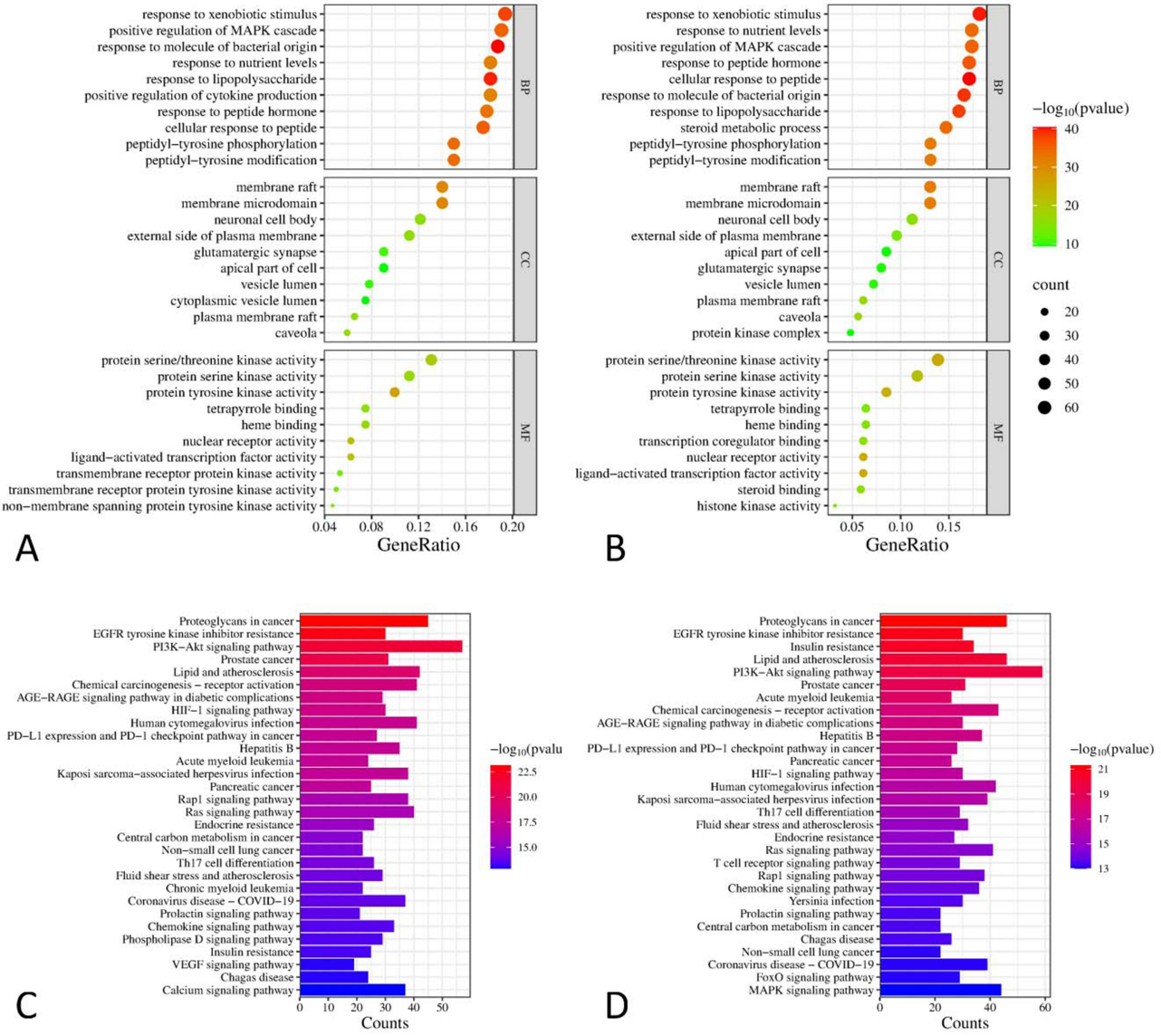

Figure 11 Functional Enrichment Analysis of Intersection Targets. (**A**) GO analysis of potential targets for chronic diarrhea treatment associated with in vivo TLG5 chemical components (TOP10). (**B**) GO analysis of potential targets for chronic diarrhea and inflammation treatment associated with in vivo TLG5 chemical components (TOP10). (**C**) KEGG analysis of potential targets for chronic diarrhea treatment associated with in vivo TLG5 chemical components (TOP30). (**D**) KEGG analysis of potential targets for chronic diarrhea and inflammation treatment associated with in vivo TLG5 chemical components (TOP30).

KEGG enrichment analysis revealed 191 pathways, including PI3K-Akt, AGE-RAGE, Ras, T-cell receptor, and MAPK. Additionally, the top 10 GO terms and 30 KEGG pathways enriched in the 376 genes were extracted. Network visualization was conducted using a clustering analyzer (Figures 11C and D).

Molecular Docking

The key targets (HSP90AA1, AKT1, STAT3, MAPK1, and ESR1) were subjected to molecular docking with five active components identified from TLG5: ferulic acid, alpha-onocerin, retinol, lignan, and sitogluside (Table S12). Typically, an absolute value of docking affinity > 4.25 indicates moderate activity, > 5.0 suggests good binding affinity, and > 7.0 represents indicative of strong binding activity. Based on this, the top five docking conformations were HSP90AA1 vs alpha-onocerin, AKT1 vs sitogluside, STAT3 vs alpha-onocerin, MAPK1 vs sitogluside, and ESR1 vs sitogluside. The results were visualized using Pymol software (Figures 12A–E).

https://doi.org/10.2147/DDDT.S527657

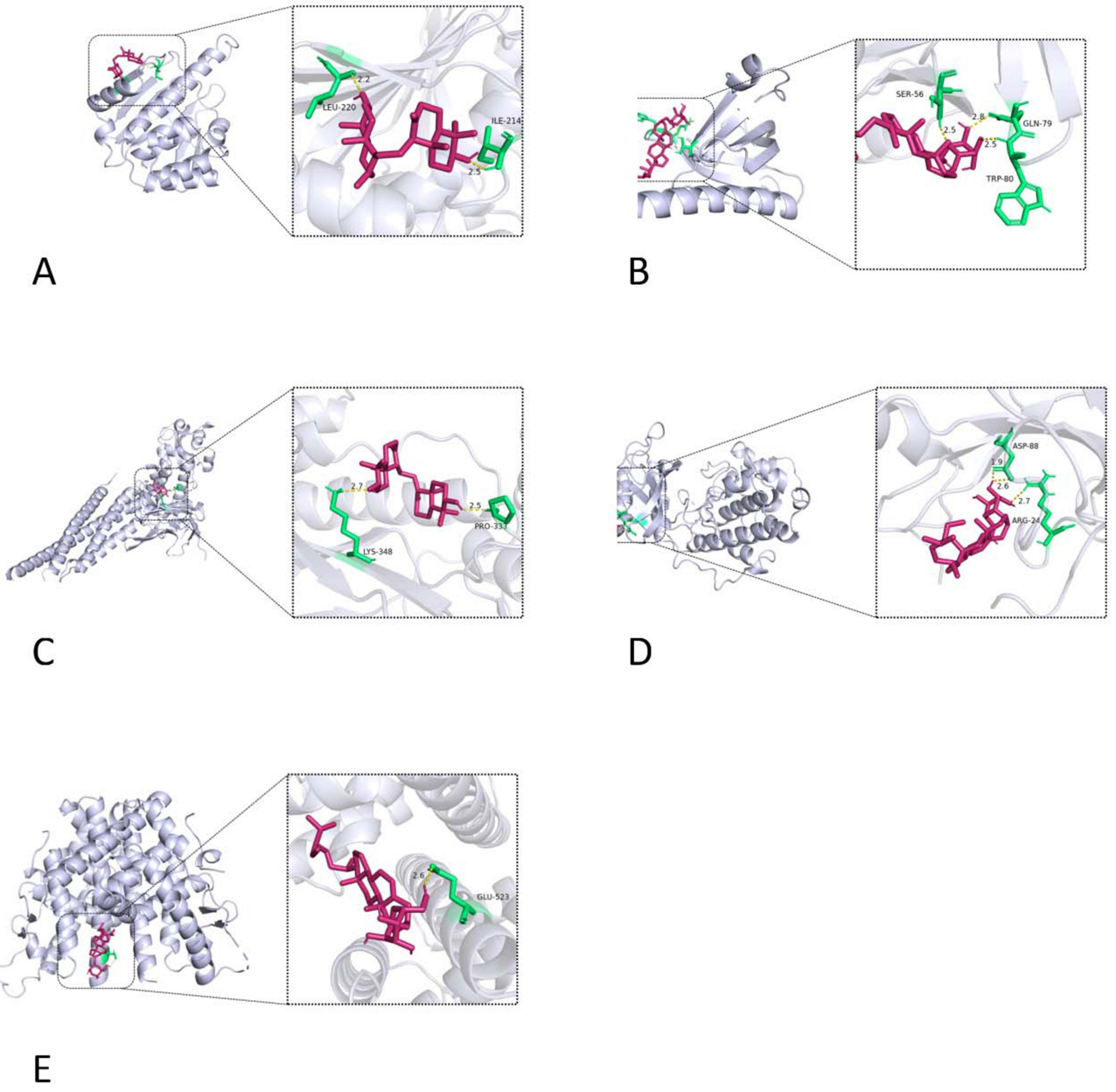

Figure 12 Molecular Docking Results of In Vivo Active Components with Core Targets. (**A**) Molecular docking of HSP90AA1 and alpha-Onocerin. (**B**) Molecular docking of AKT1 and sitogluside. (**C**) Molecular docking of STAT3 and alpha-onocerin. (**D**) Molecular docking of MAPK1 and sitogluside. (**E**) Molecular docking of ESR1 and sitogluside. **Note**: Stick models represent the active molecules, with the green stick structures corresponding to the carbon backbone of small molecules, red spheres denoting oxygen atoms, white spheres signifying hydrogen atoms, and dashed lines representing the chemical bonds between the active compounds and amino acid residues.

Transcriptomic Analysis of the Anti-Inflammatory Effects of TLG5

KEGG enrichment analysis of DEGs disclosed significant differences in inflammation-related signaling pathways between the model and control groups. The model group presented upregulated DEGs enriched in multiple inflammation-associated pathways, including primary immunodeficiency, adult T-cell leukemia, the intestinal immune network involved in IgA production, cell adhesion molecules, systemic lupus erythematosus, Th17 cell differentiation, chemokine signaling pathway, NF-kappa B signaling pathway, inflammatory bowel disease, IL-17 signaling pathway, lipid metabolism and atherosclerosis, and PI3K-Akt signaling pathway. In contrast, TLG5 treatment effectively inhibited the activation of these inflammation-associated pathways (Figures 13A and B).

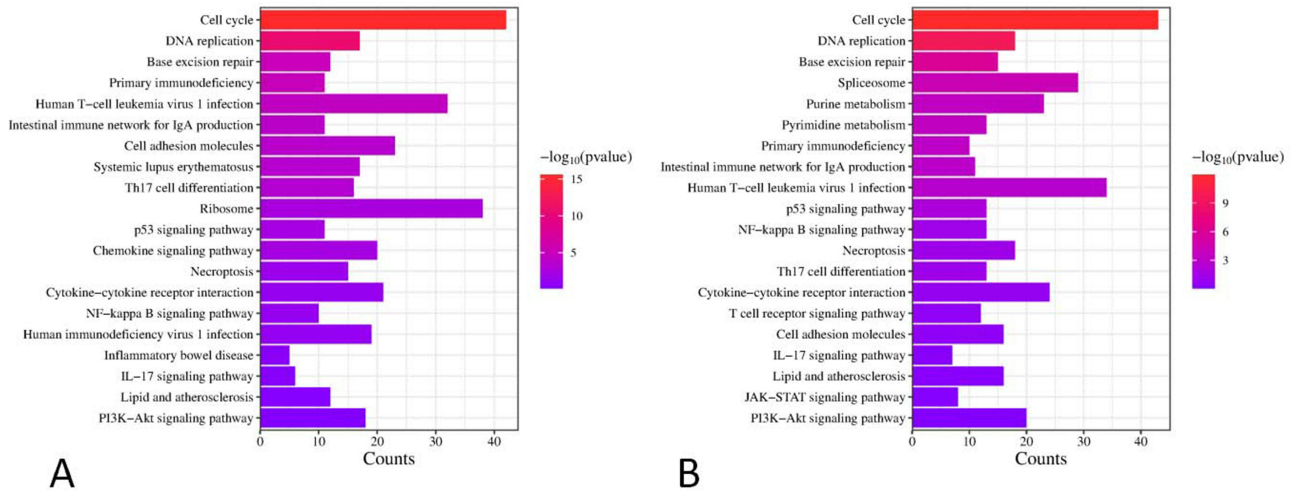

Figure 13 Transcriptomic Analysis of Colon Tissues in Rats with Chronic Diarrhea Treated with TLG5. (**A**) KEGG enrichment analysis of upregulated DEGs in the control and model groups (TOP 20). (**B**) KEGG enrichment analysis of downregulated DEGs in the model and TLG5 treatment groups (TOP 20).

In Vivo Validation of the Impact of TLG5 on Inflammation

Analysis of Serum Inflammatory Cytokines

Inflammation is one crucial etiology of chronic diarrhea. This study measured the levels of key inflammatory cytokines in the serum of experimental rats. The model group displayed elevated levels of inflammatory cytokines, including IL-1β, IL-6, and TNF-α. This denotes acute inflammatory responses triggered by the high-lactose diet. Upon TLG5 treatment, evident reductions in TNF-α and IL-1β levels were observed, while IL-6 levels showed a slight decrease below statistical significance. These findings demonstrate that TLG5 can effectively alleviate inflammatory responses triggered by high lactose intake. The efficacy is more profound in reducing TNF-α and IL-1β levels (Figures 14A–C).

Impact of TLG5 on the Expression of Intestinal Inflammatory Cytokines

The experimental findings indicated that the expression of inflammatory cytokines (TNF-α, IL-6, and IL-1β) in the colon tissues of the model group was substantially elevated compared to the control group. This suggests that high lactose intake may intensify intestinal inflammatory responses. However, upon TLG5 treatment, TNF-α, IL-6, and IL-1β levels were evidently reduced ($p < 0.05$) (Figures 14D–F).

Discussion

Chronic diarrhea is a prevalent gastrointestinal disorder, often occurring alongside conditions such as irritable bowel syndrome and inflammatory bowel disease. This condition results in persistent abnormal bowel movements lasting more than a month, significantly diminishing the quality of life of affected individuals.[21–23] The etiology of chronic diarrhea is multifactorial, potentially arising from drug reactions, underlying diseases, infections, or post-surgical consequences.[24–26] Pathophysiologically, factors such as dysbiosis, intestinal barrier dysfunction, immune-inflammatory responses, indigestion, and malnutrition interact to contribute to the onset and progression of chronic diarrhea.[27–29] Lactose, a non-absorbable sugar, enters the intestinal tract, where it undergoes fermentation, producing gas and short-chain fatty acids. This process promotes osmotic pressure within the intestinal lumen, leading to diarrhea.[26] Additionally, lactose intolerance is a prevalent food sensitivity, particularly common in specific populations.

TLG5, as a traditional Mongolian medicinal preparation, is renowned for its therapeutic effects, including promoting digestion, alleviating stagnation, and warming the stomach. Clinically, it is widely used to treat conditions such as anorexia, indigestion, cold-induced pain in the epigastric region, bloating, and diarrhea, with demonstrated efficacy.[11,12] Despite its broad clinical usage, the underlying mechanisms of its therapeutic effects on diarrhea have not been fully elucidated.

https://doi.org/10.2147/DDDT.S527657

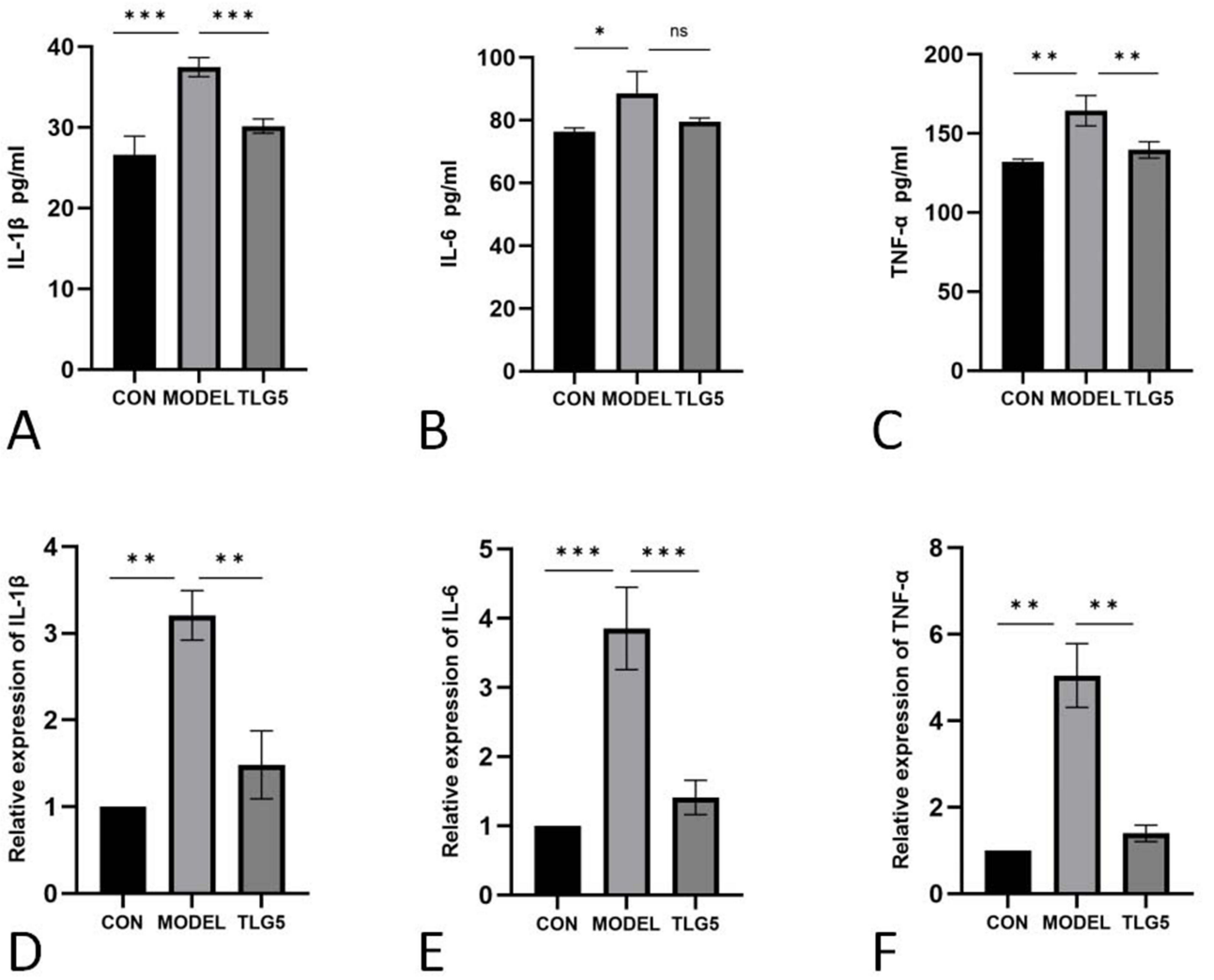

Figure 14 Inhibitory Effects of TLG5 on Inflammatory Cytokines Expression. (A)The level of inflammatory cytokine IL-1β. (**B**) The level of inflammatory cytokine IL-6. (**C**) The level of inflammatory cytokine TNF-α. (**D**) Expression of IL-1β mRNA in intestinal tissue. (**E**) Expression of IL-6 mRNA in intestinal tissue. (**F**) Expression of TNF-αmRNA in intestinal tissue.

Notes: Data are expressed as mean ± SD (*$p < 0.05$, **$p < 0.01$, ***$p < 0.001$, ns indicates no difference).

This study built a rat model with lactose-induced chronic diarrhea and administered TLG5 treatment. Through network pharmacology analysis, molecular docking, transcriptomics, and animal validation, the therapeutic effects of TLG5 on chronic diarrhea were investigated from two perspectives: the regulation of intestinal microbiota imbalance and intestinal barrier integrity by in vitro TLG5 chemical constituents and the anti-inflammatory effects of its bioactive components upon systemic absorption. The results demonstrate that TLG5 can effectively mitigate chronic diarrhea symptoms by regulating intestinal microbiota, repairing the intestinal barrier, and suppressing inflammation. These findings suggest that TLG5 can serve as a therapeutic approach to chronic diarrhea.

Network pharmacology analysis reveals that the in vitro chemical constituents of TLG5 exhibit significant potential in addressing chronic diarrhea, intestinal microbiota dysbiosis, and intestinal barrier dysfunction, particularly through the modulation of key molecules such as STAT3, TNF, IL-6, PIK3R1, and PIK3CA. STAT3, a critical transcription factor, plays an essential role in cell proliferation, apoptosis, and the self-repair of epithelial.[30,31] Existing research has demonstrated that STAT3 stabilizes the intestinal barrier by inhibiting inflammatory cytokines and promoting the expression of anti-inflammatory mediators.[8,32] Additionally, TNF and IL-6, as pivotal inflammatory cytokines, are implicated in chronic diarrhea and the integrity of the intestinal barrier. Modulation of these cytokines has been shown to effectively reduce intestinal inflammation, presenting a promising approach to chronic diarrhea management.[33]

PIK3R1 and PIK3CA, integral components of the PI3K-AKT signaling pathway, are not directly targeted in chronic diarrhea. However, the pathway facilitates intestinal homeostasis by indirectly promoting cell survival and proliferation via AKT1 activation.[34,35] The in vitro components of TLG5, associated with intestinal microbiota dysbiosis and intestinal barrier impairment, appear to regulate key targets (eg, TNF, NFKB1, and IL1B), thereby ameliorating intestinal function. This observation is consistent with previous studies, which underscore the critical roles of these targets in maintaining intestinal microbiota balance and immune homeostasis via IL-17 and TNF signaling pathways.[36,37] These findings suggest that TLG5 likely exerts its therapeutic effects via multiple signaling pathways to maintain the health and metabolic equilibrium of intestinal microbiota.

Transcriptomic analysis further corroborates these results, revealing that TLG5 significantly activates pathways associated with chronic diarrhea and intestinal microbiota dysbiosis. Notably, the activation of bile secretion and mineral absorption pathways suggests an enhancement in intestinal microbiota metabolic activity.[38,39] Bile acids, as major constituents of bile, directly influence both the structure and function of intestinal microbiota. This provides deeper insights into the underlying mechanisms of TLG5, reinforcing its therapeutic potential for improving intestinal health.

The findings from 16S rRNA sequencing validate the transcriptomic results. TLG5 treatment notably increases bacterial diversity, inhibits pathogenic bacteria, and enhances the abundance of short-chain fatty acid-producing genera, such as *Bifidobacterium* and *Coriobacteriaceae* UCG-002. These results align with the transcriptomic pathway enrichment data, forming a coherent body of evidence. The in vivo experimental outcomes also strongly support these findings.

In the chronic diarrhea model, levels of bile acids and SCFAs were significantly downregulated, whereas TLG5 treatment resulted in a remarkable increase in these metabolites. This result substantiates the potential of TLG5 in modulating intestinal microbiota and improving the intestinal environment. Additionally, the in vitro chemical components of TLG5 were found to be closely associated with 126 targets implicated in intestinal barrier dysfunction, emphasizing the critical roles of STAT3 and TNF in preserving the integrity of the intestinal barrier.

Transcriptomic analysis showed that the therapeutic effects of TLG5 on intestinal barrier function were likely achieved through the upregulation of multiple signaling cascades, including focal adherence, adherens junction, ECM-receptor interaction, MAPK, and TGF-β. The activation of these pathways is directly involved in stabilizing and repairing the intestinal barrier.[40,41] Specifically, the activation of focal adherence and adherens junction facilitates strengthening epithelial cell connections, preventing the infiltration of hazardous substances, and preserving intestinal barrier integrity. ECM-receptor interaction provides essential support for epithelial cell survival and proliferation, thereby reinforcing intestinal barrier integrity. MAPK and TGF-β signaling pathways play pivotal roles in regulating cell growth, apoptosis, and inflammation, contributing to the repair and stabilization of the intestinal barrier.[42,43.]

In vivo validation corroborated these findings. TLG5 significantly alleviated diarrhea symptoms induced by a high-lactose diet and promoted the restoration of intestinal function, which was closely tied to the enhancement of intestinal barrier integrity. Histological assessments demonstrated that TLG5 treatment remarkably upregulated the expression of tight junction proteins, such as Claudin and Occludin, in colonic tissue, indicative of improved intestinal barrier function. Furthermore, inflammatory cytokines (TNF-α, IL-1β, and IL-6) in the colonic tissue of TLG5-treated rats were profoundly reduced, confirming the anti-inflammatory effects of TLG5 and subsequent alleviation of intestinal barrier damage. Additional molecular docking analysis validated the strong binding affinity of TLG5 active components with key targets, including STAT3, AKT1, and NFKB1.

Simultaneously, TLG5 exhibits significant anti-inflammatory effects through its bioactive components, improving symptoms of chronic diarrhea. Network pharmacology analysis identified 34 active constituents in TLG5, from which a target dataset was constructed, encompassing 32 bioactive compounds and 638 associated targets. This underscores the pivotal role of network pharmacology in elucidating the mechanistic pathways of drug action. The pathogenesis of chronic diarrhea is multifactorial, with inflammation as a central factor.[44,45] Through database retrieval, 1841 inflammation-related targets were identified. The intersection analysis with TLG5 targets revealed 321 chronic diarrhea-associated targets and 212 potential targets. These findings suggest that TLG5 not only impacts intestinal targets but also modulates systemic inflammatory processes. In the key target screening, STAT3 and HSP90AA1 were highlighted as crucial not only in the pathogenesis of diarrhea but also as regulators of inflammation.[46–48] Functional enrichment analysis highlighted that the intersection targets of TLG5 were predominantly involved in KEGG pathways related to inflammation

and stress responses, suggesting that TLG5 exerts its anti-inflammatory effects by modulating these pathways. Molecular docking analysis revealed the strong binding affinity between TLG5 active compounds and key targets, while transcriptomic analysis demonstrated that TLG5 effectively inhibited the activation of inflammatory signaling pathways. In vivo validation substantiated that TLG5 significantly reduced serum levels of inflammatory cytokines, providing robust evidence of its anti-inflammatory effects.

For the symptomatic treatment of chronic diarrhea, drugs such as gel-forming fibers and cholestyramine have demonstrated some utility, although they also present certain limitations.[5,49] Racecadotril, an enkephalinase inhibitor approved for acute diarrhea, has limited long-term data for chronic diarrhea, and its long-term efficacy and safety remain obscure. Emerging therapies, such as Eluxadolin, alleviate abdominal pain and diarrhea by modulating opioid receptors in the intestinal nervous system. However, their mechanism of action is relatively narrow.[50,51] For refractory irritable bowel syndrome with diarrhea (IBS-D), treatments, including 5-HT3 receptor antagonists, rifaximin, and low-dose tricyclic antidepressants, show some effects but are often hindered by significant individual variability and poor efficacy in certain patients.[52] Specific dietary interventions, such as a low FODMAP diet, can help mitigate IBS symptoms, but these require long-term patient adherence and may not be effective for all individuals.[53]

In the lactose-induced chronic diarrhea rat model used in this study, TLG5 evidently alleviated diarrhea symptoms and promoted the recovery of intestinal function. This finding suggests that TLG5 not only effectively controls diarrhea symptoms but may also exert its effects through multiple mechanisms. Specifically, first, TLG5 regulates the intestinal microbiota, ameliorating microbial imbalance and creating a healthier microecological environment in the intestine; second, it repairs the intestinal barrier, enhancing its function and preventing harmful substances from entering intestinal tissues; third, it inhibits inflammatory responses, thereby reducing intestinal inflammation. Through these multifaceted mechanisms, TLG5 fundamentally improves the pathological state of the intestine, offering a more durable therapeutic effect and presenting a novel perspective and approach for the management of chronic diarrhea.

Despite the remarkable results of this study, certain limitations still exist. First, the effect of TLG5 on intestinal flora is a complex process, and its specific mechanism of action and targets need to be further explored. In addition, experiments are needed to clarify the specific effects of intestinal flora metabolites on the intestinal barrier in mice with chronic diarrhea. Future research directions should include the long-term regulatory mechanisms of TLG5 on the intestinal flora and the use of macro-genomics and other technologies to reveal the profound effects of TLG5 on the structure and function of microbial communities. Meanwhile, the combined efficacy of TLG5 with other therapeutic approaches, such as with probiotics or other anti-inflammatory drugs, should also be explored, and the synergistic effect should be evaluated. In addition, future studies should focus on the comprehensive effects of long-term use of TLG5 on intestinal health, especially the long-term stability of intestinal barrier function, immune response, and microbial ecological balance.

Conclusion

This study delved into the therapeutic effects and molecular mechanisms of the traditional Mongolian medicine TLG5 in the context of lactulose-induced diarrhea. The results indicate that TLG5 can alleviate chronic diarrhea symptoms by restoring the balance of intestinal microbiota, ameliorating intestinal barrier function, and suppressing inflammation. These findings demonstrate that TLG5 represents a promising therapeutic agent for chronic diarrhea.

Abbreviations

TLG5, Tonglaga-5; UPLC-Q/TOF MS^E, Ultra performance liquid chromatography-quadrupole/time of flight MS^E; SD, Sprague-Dawley; PCR, Polymerase Chain Reaction; qPCR, Quantitative polymerase chain reaction; RT-PCR, Real-time quantitative polymerase chain reaction; ELISA, Enzyme linked immunosorbent assay; SCFAs, Short-chain fatty acids; STAT3, Signal transducer and activator of transcription 3; TNF, Tumor necrosis factor; IL-6, Interleukin-6; IL-17, Interleukin-17; PIK3R1, Phosphoinositide-3-kinase regulatory subunit 1; PIK3CA, Phosphatidylinositol-4,5-bisphosphate 3-kinase catalytic; PIK3CB, Phosphatidylinositol-4,5-Bisphosphate 3-Kinase Catalytic Subunit Beta; HSP90AA1, Heat shock protein 90 alpha family class a member 1; AKT1, AKT serine/threonine kinase 1; MAPK1, Mitogen-activated protein kinase 1; ESR1, Estrogen receptor 1; DEGs, differentially expressed genes; F/B, Firmicutes-

to-bacteroidetes; ZO-1, Zona occludens 1; IL-1β, Interleukin-1beta; TNF-α, Tumour necrosis factor-alpha; 5-HT3, 5-hydroxytryptamine type 3; ESI, electrospray ionization; TCMSP, Traditional Chinese medicine systems pharmacology database; OMIM, Online Mendelian inheritance in man; PPI, Protein-protein interaction; GO, Gene ontology; KEGG, Kyoto encyclopedia of genes and genomes; PDB, Protein data bank; OD, Optical density; HE, Hematoxylin-eosin; PBS, Phosphate buffer saline; BSA, bovine serum albumin; DAB, Diaminobenzidine; QIIME2, Quality Interactive Metadata Inference Environment 2; UPGMA, Unweighted pair-group method with arithmetic means; HISAT2, Hierarchical Indexing for Spliced Alignment of Transcripts 2; FPKM, Fragments Per Kilobase per Million; GSEA, Gene set enrichment analysis; HRP, horseradish peroxidase; TIC, Total Ion Chromatogram; STRING, search tool for recurring instances of neighbouring genes; TP53, Tumor protein p53; SRC, SRC proto-oncogene, non-receptor tyrosine kinase; NFKB1, Nuclear factor kappa B subunit 1; TLR2, Toll like receptor 2; RELA, RELA proto-oncogene, NF-KB subunit; BP, Biological processes; CC, Cellular component; MF, Molecular function; AGE-RAGE, Advanced glycation end products-receptor for advanced glycosylation end products; PI3K-Akt, Phosphatidylinositol 3 kinase -protein kinase B; ECM, Extracellular matrix; TGF-β, Transforming growth factor beta; PPAR, Peroxisome proliferators-activated receptor; PCoA, Principal co-ordinates analysis; NF-kappa B, Nuclear factor-kappa B.

Acknowledgments

We sincerely extend our gratitude to the Mongolian Medicine Processing Experiment Center and the Mongolian Medicine Basic Experiment Center at the School of Mongolian Medicine, Inner Mongolia Medical University, for providing the experimental platform for this research. Supported by Program for Innovative Research Team in Universities of lnner Mongolia Autonomous Region (Grant number: NMGIRT2418); Supported By Program for Young Talents of Science and Technology in Universities of Inner Mongolia Autonomous Region (Grant number: NJYT23052); the first-class discipline research project (Grant number: YLXKZX-NYD-009); the general project of Inner Mongolia Medical University (Grant number: YKD2022MS006 and YKD2023MS062); the key project of Inner Mongolia Medical University (Grant number: YKD2022ZD008); the Duxue Talent Program of Inner Mongolia Medical University (Grant number: ZY20243102); the Natural Science Foundation of Inner Mongolia (Grant number: 2023MS08050, 2024MS08054, and 2024LHMS08024); the research capacity enhancement project for graduate students in Mongolian medicine at Inner Mongolia Medical University (Grant number: Myx2022-R14).

Author Contributions

All authors contributed significantly to the work presented, including the conception, study design, execution, data acquisition, analysis, and interpretation. Each author participated in drafting, revising, or critically reviewing the manuscript. All authors gave final approval of the version to be published, agreed on the journal to which the article has been submitted, and are accountable for all aspects of the work.

Disclosure

The authors declare that they have no known competing financial interests or personal relationships that could have appeared to influence the work reported in this paper.

References

1. Tack J. Functional diarrhea. *Gastroenterol Clin North Am*. 2012;41(3):629–637. doi:10.1016/j.gtc.2012.06.007
2. Choung RS, Locke GR 3rd, Schleck CD, Zinsmeister AR, Talley NJ. Cumulative incidence of chronic constipation: a population-based study 1988-2003. *Aliment Pharmacol Ther*. 2007;26(11–12):1521–1528. doi:10.1111/j.1365-2036.2007.03540.x
3. Brum JM, Gibb RD, Ramsey DL, Balan G, Yacyshyn BR. Systematic review and meta-analyses assessment of the clinical efficacy of bismuth subsalicylate for prevention and treatment of infectious diarrhea. *Dig Dis Sci*. 2021;66(7):2323–2335. doi:10.1007/s10620-020-06509-7
4. Lee KJ. Pharmacologic Agents for Chronic Diarrhea. *Intest Res*. 2015;13(4):306–312. doi:10.5217/ir.2015.13.4.306
5. Ulbricht K, Layer P, Andresen V. Diagnostik und Therapie der chronischen nicht-infektiösen Diarrhö (Chronic, non-infectious diarrhea: diagnostics and therapy). *Dtsch Med Wochenschr*. 2016;141(19):1395–1402. doi:10.1055/s-0042-108700
6. Nee J, Zakari M, Lembo AJ. Current and emerging drug options in the treatment of diarrhea predominant irritable bowel syndrome. *Expert Opin Pharmacother*. 2015;16(18):2781–2792. doi:10.1517/14656566.2015.1101449

7. Graven-Nielsen CS, Knoph CS, Okdahl T, et al. Opioids in the treatment of chronic idiopathic diarrhea in humans-a systematic review and treatment guideline. *J Clin Med*. 2023;12(7):2488. doi:10.3390/jcm12072488
8. Xu Z, Zhang Q, Ding C, et al. Beneficial effects of hordenine on a model of ulcerative colitis. *Molecules*. 2023;28(6):2834. doi:10.3390/molecules28062834
9. Tian Y, Fu M, Su J, et al. Gut microbiota dysbiosis and intestinal barrier impairment in diarrhea caused by cold drink and high-fat diet. *Toxicology*. 2024;502:153728. doi:10.1016/j.tox.2024.153728
10. Luo Q, Lei X, Xu J, et al. An altered gut microbiota in duck-origin parvovirus infection on cherry valley ducklings is associated with mucosal barrier dysfunction. *Poult Sci*. 2021;100(4):101021. doi:10.1016/j.psj.2021.101021
11. Chen X, Zhang H, Wang X, Tai W. Sugemule-10: source of prescription and modern clinical application. *Chin Herb Med*. 2022;14(3):376–384. doi:10.1016/j.chmed.2022.06.006
12. Zhang C-H, Zhang N. Research progress of Mongolian medicine digeda. *Zhongguo Zhong Yao Za Zhi*. 2013;38(24):4362–4368.
13. Fürst R, Zirrgiebel U, Totzke F, Zahler S, Vollmar AM, Koch E. The Crataegus extract WS 1442 inhibits balloon catheter-induced intimal hyperplasia in the rat carotid artery by directly influencing PDGFR-beta. *Atherosclerosis*. 2010;211(2):409–417. doi:10.1016/j.atherosclerosis.2010.04.003
14. Gao J, Li J, An Y, et al. Increasing effect of Tangzhiqing formula on IRS-1-dependent PI3K/AKT signaling in muscle. *BMC Complement Altern Med*. 2014;14:198. doi:10.1186/1472-6882-14-198
15. Dilek NM, Babaoğlu AS, Unal K, Ozbek C, Pırlak L, Karakaya M. Marination with aronia, grape and hawthorn vinegars affects the technological, textural, microstructural and sensory properties of spent chicken meat. *Br Poult Sci*. 2023;64(3):357–363. doi:10.1080/00071668.2022.2163616
16. Yu Q, Zhu L, Ding X, Lou Y. Integration of network pharmacology and experimental validation to explore the pharmacological mechanism of andrographolide against asthma. *Bioresour Bioprocess*. 2025;12(1):30. doi:10.1186/s40643-025-00869-6
17. Ma JX, Chen T, Xue H, et al. Jian-Pi-Yin decoction attenuates lactose-induced chronic diarrhea in rats by regulating GLP-1 and reducing NHE3 ubiquitination and phosphorylation. *Heliyon*. 2023;9(7):e17444. doi:10.1016/j.heliyon.2023.e17444
18. Boakye PA, Brierley SM, Pasilis SP, Balemba OB. Garcinia buchananii bark extract is an effective anti-diarrheal remedy for lactose-induced diarrhea. *J Ethnopharmacol*. 2012;142(2):539–547. doi:10.1016/j.jep.2012.05.034
19. Singh VK, Seed TM. Entolimod as a radiation countermeasure for acute radiation syndrome. *Drug Discov Today*. 2021;26(1):17–30. doi:10.1016/j.drudis.2020.10.003
20. DeLuca DS, Levin JZ, Sivachenko A, et al. RNA-SeQC: RNA-seq metrics for quality control and process optimization. *Bioinformatics*. 2012;28(11):1530–1532. doi:10.1093/bioinformatics/bts196
21. Sarowska J, Choroszy-Król I, Regulska-Ilow B, Frej-Mądrzak M, Jama-Kmiecik A. The therapeutic effect of probiotic bacteria on gastrointestinal diseases. *Adv Clin Exp Med*. 2013;22(5):759–766.
22. Walsham NE, Sherwood RA. Fecal calprotectin in inflammatory bowel disease. *Clin Exp Gastroenterol*. 2016;9:21–29. doi:10.2147/CEG.S51902
23. Koloski N, Shah A, Kaan I, et al. Healthcare utilization patterns: irritable bowel syndrome, inflammatory bowel disease, and gastroesophageal reflux disease. *Dig Dis Sci*. 2024;69(5):1626–1635. doi:10.1007/s10620-024-08297-w
24. Repin I, Avetisian AO, El'kin AV, Otten TF, Riasnianskaia TE, Trofimov MA. Znachenie lekarstvennoĭ ustoĭchivosti mikobakteriĭ v khirurgii tuberkuleza legkikh (Significance of mycobacterial drug resistance in pulmonary tuberculosis surgery). *Probl Tuberk*. 2001;9:6–10.
25. Sellner J, Trinka E. Clinical characteristics, risk factors and pre-surgical evaluation of post-infectious epilepsy. *Eur J Neurol*. 2013;20(3):429–439. doi:10.1111/j.1468-1331.2012.03842.x
26. Chioma OS, Wiggins Z, Rea S, Drake WP. Infectious and non-infectious precipitants of sarcoidosis. *J Autoimmun*. 2024;149:103239. doi:10.1016/j.jaut.2024.103239
27. Ramamurthy T, Kumari S, Ghosh A. Diarrheal disease and gut microbiome. *Prog Mol Biol Transl Sci*. 2022;192(1):149–177.
28. Philips CA, Augustine P. Gut barrier and microbiota in cirrhosis. *J Clin Exp Hepatol*. 2022;12(2):625–638. doi:10.1016/j.jceh.2021.08.027
29. Son M, Park IS, Kim S, et al. Novel potassium-competitive acid blocker, tegoprazan, protects against colitis by improving gut barrier function. *Front Immunol*. 2022;13:870817. doi:10.3389/fimmu.2022.870817
30. Duan Z, Bradner JE, Greenberg E, et al. SD-1029 inhibits signal transducer and activator of transcription 3 nuclear translocation. *Clin Cancer Res*. 2006;12(22):6844–6852. doi:10.1158/1078-0432.CCR-06-1330
31. Qi QR, Yang ZM. Regulation and function of signal transducer and activator of transcription 3. *World J Biol Chem*. 2014;5(2):231–239. doi:10.4331/wjbc.v5.i2.231
32. Shao X, Li J, Shao Q, et al. Water-soluble garlic polysaccharide (WSGP) improves ulcerative volitis by modulating the intestinal barrier and intestinal flora metabolites. *Sci Rep*. 2024;14(1):21504. doi:10.1038/s41598-024-72797-y
33. Gu J, Hu J, Qian H, et al. Intestinal barrier dysfunction: a novel therapeutic target for inflammatory response in acute stanford type A aortic dissection. *J Cardiovasc Pharmacol Ther*. 2016;21(1):64–69. doi:10.1177/1074248415581176
34. Cizkova M, Vacher S, Meseure D, et al. PIK3R1 underexpression is an independent prognostic marker in breast cancer. *BMC Cancer*. 2013;13:545. doi:10.1186/1471-2407-13-545
35. Yu Y, Savage RE, Eathiraj S, et al. Targeting AKT1-E17K and the PI3K/AKT pathway with an allosteric AKT inhibitor, ARQ 092. *PLoS One*. 2015;10(10):e0140479. doi:10.1371/journal.pone.0140479
36. Hernández-Chirlaque C, Aranda CJ, Ocón B, et al. Germ-free and antibiotic-treated mice are highly susceptible to epithelial injury in DSS colitis. *J Crohns Colitis*. 2016;10(11):1324–1335. doi:10.1093/ecco-jcc/jjw096
37. Zhao H, Wang Q, Zhao J, et al. Ento-A alleviates DSS-induced experimental colitis in mice by remolding intestinal microbiota to regulate SCFAs metabolism and the Th17 signaling pathway. *Biomed Pharmacother*. 2024;170:115985. doi:10.1016/j.biopha.2023.115985
38. Zhang Z, Huang B, Wang Y, Zhan Y, Zhu M, Wang C. Dynamic alterations in the donkey fecal bacteria community and metabolome characteristics during gestation. *Front Microbiol*. 2022;13:927561. doi:10.3389/fmicb.2022.927561
39. Tang Z, Zhan L, He R, et al. Hepatoprotective effect of tea composite solid beverage on alcohol-caused rat liver injury. *Foods*. 2023;12(22):4126. doi:10.3390/foods12224126

40. Wong CH, Cheng CY. Mitogen-activated protein kinases, adherens junction dynamics, and spermatogenesis: a review of recent data. *Dev Biol*. 2005;286(1):1–15. doi:10.1016/j.ydbio.2005.08.001
41. Zhu X, Wang J, Jin X, Chen Y, Hu L, Zhao J. Construction and evaluation of a prognostic risk assessment model of gastric cancer by using hypoxia features. *Mutat Res*. 2022;825:111795. doi:10.1016/j.mrfmmm.2022.111795
42. Sturm A, Dignass AU. Epithelial restitution and wound healing in inflammatory bowel disease. *World J Gastroenterol*. 2008;14(3):348–353. doi:10.3748/wjg.14.348
43. Mortensen JH, Lindholm M, Langholm LL, et al. The intestinal tissue homeostasis - the role of extracellular matrix remodeling in inflammatory bowel disease. *Expert Rev Gastroenterol Hepatol*. 2019;13(10):977–993. doi:10.1080/17474124.2019.1673729
44. El-Salhy M, Gundersen D, Hatlebakk JG, Hausken T. Clinical presentation, diagnosis, pathogenesis and treatment options for lymphocytic colitis (Review). *Int J Mol Med*. 2013;32(2):263–270. doi:10.3892/ijmm.2013.1385
45. Vyas SP, Goswami R. A decade of Th9 cells: role of Th9 CELLS IN INFLAMMATORY BOWEL DISEAse. *Front Immunol*. 2018;9:1139. doi:10.3389/fimmu.2018.01139
46. Jiang C, Yang H, Chen X, et al. Macleaya cordata extracts exert antiviral effects in newborn mice with rotavirus-induced diarrhea via inhibiting the JAK2/STAT3 signaling pathway. *Exp Ther Med*. 2020;20(2):1137–1144. doi:10.3892/etm.2020.8766
47. Shao R, Yang Z, Zhang W, et al. Pachymic acid protects against Crohn's disease-like intestinal barrier injury and colitis in mice by suppressing intestinal epithelial cell apoptosis *via* inhibiting PI3K/AKT signaling. *Nan Fang Yi Ke Da Xue Xue Bao*. 2023;43(6):935–942. doi:10.12122/j.issn.1673-4254.2023.06.08
48. Ma Z, Chen X, Xiong M, et al. Cyberpharmacology uncover the mechanism of the total Rhizoma Coptidis extracts ameliorate chronic atrophic gastritis. *J Ethnopharmacol*. 2024;335:118644. doi:10.1016/j.jep.2024.118644
49. Vohmann B, Hoffmann JC. Antidiarrhoika bei chronischer Diarrhoe [Antidiarrheal drugs for chronic diarrhea]. *Dtsch Med Wochenschr*. 2013;138(45):2309–2312. doi:10.1055/s-0033-1349597
50. Cash BD, Lacy BE, Rao T, Earnest DL. Rifaximin and eluxadoline - newly approved treatments for diarrhea-predominant irritable bowel syndrome: what is their role in clinical practice alongside alosetron? *Expert Opin Pharmacother*. 2016;17(3):311–322. doi:10.1517/14656566.2016.1118052
51. Foxx-Orenstein AE. New and emerging therapies for the treatment of irritable bowel syndrome: an update for gastroenterologists. *Therap Adv Gastroenterol*. 2016;9(3):354–375. doi:10.1177/1756283X16633050
52. Piovezani Ramos G, Camilleri M. Current and future therapeutic options for irritable bowel syndrome with diarrhea and functional diarrhea. *Dig Dis Sci*. 2023;68(5):1677–1690. doi:10.1007/s10620-022-07700-8
53. Patel NV. "Let food be thy medicine": diet and supplements in irritable bowel syndrome. *Clin Exp Gastroenterol*. 2021;14:377–384. doi:10.2147/CEG.S321054